AMELIORATION OF STRESS CONCENTRATIONS BY MATERIAL REMOVAL

A Thesis

Presented to

The Faculty of Graduate Studies and Research

THE UNIVERSITY OF MANITOBA

In Partial Fulfilment

of the Requirements for the Degree

MASTER OF SCIENCE IN MECHANICAL ENGINEERING

---

by

Brij Mohan Dhand

May, 1969

SYNOPSIS

Two-dimensional photoelastic stress analysis has been employed to study the effect of stress concentrations in the vicinity of other stress concentrations.

The specimens are loaded in uni-axial tension. Two types of stress raisers are studied, one being the circular hole, and the other double symmetrical V-notches. In the vicinity of these raisers, material has been removed (stress reducers) in different amounts. The raiser is located in the mid section of shank length in all models. The stress reducer consists of a geometrical shape similar to the raiser, but its size being increased relative to the fixed size of stress raiser. A pair of similar stress reducers is arranged symmetrically beside the raiser and in the direction of loading. The effect of variation of stress reducer size, and that of pitch between raiser and each reducer has been studied. It has been found that the stress concentration keeps on reducing at the raiser while it goes on increasing at the reducer until an optimum stage is reached where the stress concentration is same at the raiser and reducer.

The results are illustrated finally with the aid of parametric curves. The investigation concludes that a definite reduction of stress concentration is possible by material removal.

ACKNOWLEDGMENTS

The author is indebted to Dr. J. Shewchuk, Associate Professor of Mechanical Engineering, thesis advisor, and to Dr. B. N. Thadani, Associate Professor of Civil Engineering, thesis co-advisor, for their valuable advice, suggestions and generous support.

The author also acknowledges the assistance of the Mechanical Engineering Department and of the machine shop technicians.

The grant of the National Research Council of Canada in aid of this research programme is acknowledged as well.

TABLE OF CONTENTS

LIST OF TABLES

LIST OF FIGURES

Figure Page

NOMENCLATURE

σ_1, σ_2	Principal Stresses.
σ_{nom}	Nominal Stress.
σ_{max}	Maximum Stress.
θ	Angle.
P	Tensile Load.
N	Fringe Order.
N_{nom}	Fringe Order Corresponding to Nominal Stress.
N_{max}	Fringe Order Corresponding to Maximum Stress.
A_g	Gross Cross-sectional Area.
A	Net Cross-sectional Area
K_t	Theoretical Stress Concentration Factor.
K_e	Effective Stress Concentration Factor.
K_f	Fatigue Stress Concentration Factor.
Δ	Relative Retardation.
c	Relative Stress Optic Co-efficient expressed in brewsters.
t or h	Uniform Thickness of Model.
f_σ	Material Fringe Value.
F	Model Fringe Value.
R, R_1, R_2, r	Radius.
B, x, a, b	Linear Distance.

SCF	Stress Concentration Factor.
σ_r	Radial Stress.
σ_θ	Tangential Stress.
$\Gamma_{r\theta}$	Shear Stress.

CHAPTER 1

INTRODUCTION

Any engineering structure or machine before manufacture must be designed according to modern principles in a most economic way, or in other words, the designed components must be mechanically strong and rigid, whilst using a minimum quantity of materials for their manufacture.

When designing such structures and machines various factors have to be taken into consideration. One of these is stress concentration around geometrical discontinuities like holes, notches and other recesses in plane and three-dimensional parts.

Because of the damaging effects of stress concentration on the fatigue life of a member, attempts have been made in modern engineering problems to relieve or reduce stress concentrations below the minimum value that will cause a fatigue fracture to occur. There are several methods of relieving stress concentrations. These are, avoiding abrupt cross-sectional change of member by use of fillets, making the portion of the member in the neighbourhood of stress concentration less stiff by material removal or substituting material of lower modulus of elasticity, and increasing fatigue strength by cold working the portions near the stress concentration.

The problem to be investigated in this thesis has been formulated from the point of view of reducing stress concentration in the

tension members with respect to two types of discontinuities, namely, holes and notches in plane stress analysis. The basis of reduction is material removal in a manner unique in itself in the sense that stress reducers in pairs are introduced symmetrically beside the stress raiser. The stress reducer is similar in geometrical shape to stress raiser but dimensionally its size being increased in comparison to the fixed size of stress raiser.

The problem of determining elastic stress concentrations in multi-connected continua is not analytically simple and, therefore, two dimensional photoelasticity is employed to study the problem.

The usefulness of the science of photoelasticity in the engineering world was first recognized by the pioneers Coker and Filon [57] at the beginning of this century and since then it has been drawing keen interest from researchers. Today, it has become an indispensable mechanical technique for stress analysts to solve varied research problems of practical interest.

Photoelasticity has the advantage of depicting an overall picture of the stress distribution and concentration. It is applicable to any state of stress, but it can most conveniently be applied to two-dimensional stress studies.

The present problem may be studied as a plane stress case on the assumption that thickness of the tension member is small in comparison to its other dimensions or there is a uniform application of the load throughout its thickness.

The fringe order at the point of stress concentration on the

boundary of the hole or notch in conjunction with the load constituted the photoelastic data. The parametric curves ultimately obtained, give an idea of percentage reduction of stress concentration effects by material removal.

CHAPTER 2

REVIEW OF LITERATURE

2.1 Introduction

This chapter deals with two different phases. In the first, the basic understanding of the phenomenon of stress concentration in general, with its effects, is described. The studies of those researchers who have worked on this phenomenon are then reviewed to some extent in the second phase, with special reference to the plane stress cases of holes and notches in uniaxial tension members.

2.2 What Is Stress Concentration?

Basically, the stresses in loaded members are determined by simple mathematical formulas, based on the assumptions particular to the type of loading, together with the well known Saint - Venant's Principle [1]. For example, in a tension member subjected to an axial load, the stress is assumed to be distributed uniformly over each cross-section; in a beam the stress on each cross section is assumed to increase directly (elastic case) with the distance from the neutral axis. But, under some conditions the stress at the point considered may be radically different from the value calculated using the ordinary formulas. The condition that causes the stresses to be greater is the presence of discontinuities or stress raisers or stress concentrators. Various discontinuities occur in

practice, which destroy the assumed regularity of the stress distribution by sudden increases in the stress at points near the stress raiser, thus causing the plane cross-sections not to remain plane.

Hence stress concentration is the well known increase in the localized stress or the maximum stress or the peak stress developed, as a rule, in only a small portion of the member mainly due to geometrical discontinuities such as holes, notches, grooves, corners and sudden changes of the cross-section etc., in mechanically loaded members.

Sometimes, stress concentration also results from discontinuities in the material itself, such as non-metallic inclusions in steel, air holes in concrete etc. There are few other causes of stress concentration. One may be the variations in the strength and stiffness of the component elements of which the member is made, such as crystalline grains in steel, ingredients in concrete. Another is the initial stresses in the member due, for instance, to overstraining and cold working of metals during erection or fabrication, to heat treatment of metals, to shrinkage in castings and in concrete. Stress concentrations can also occur due to residual stresses resulting from welding operations.

2.3 Importance of Stress Concentration

Stress concentrations are of particular interest to machine designers, especially when concerned with the important modern engineering questions of fatigue and fracture of materials. In fatigue conditions, the normal endurance limit of member is markedly reduced because of stress raisers by a factor approximately equal to the factor of stress concentra-

tion even though the material be quite ductile.

The investigations of A. Wöhler [2] by a series of systematic fatigue tests on railway axles in the last century were actually one of the first considerations of stress concentration. Wöhler detected the detrimental influence of sudden changes of cross-section on the strength, especially for repeated loading. The basic tests by Wöhler were continued later by Bauschinger and A. Föpple [3] at the Technical University, Munich.

The first application of a stress concentration result for the theoretical treatment of fracture in brittle solids was made by Griffith [4]. He took an elliptic hole in a flat plate as a model for a crack and derived a critical stress value for which an existing crack will propogate.

The consistent trend in aircraft design toward higher speeds, larger sizes, and higher wing loading combine to make the problem of stress concentrations also of importance in this field. The high stress concentration at the edge of a hole is of much practical importance, for example, in the problems of flows in otherwise continuous material and in holes in ship's decks and airplane fuselages.

The general significance of stress concentration in machines or other structural components subjected to fatigue is, therefore, well established. As a result, this aroused the attention of many investigators who tried to define and understand the phenomena. The stress distribution around various types of geometrical discontinuities and its effect on strength has already been studied. Some tried to reduce the stress concentration effect thus improving fatigue strength. In the remainder of this chapter, some of the studies of those scientists who

have contributed to the research in the field of stress concentration are reviewed.

2.4 Review of Previous Research

An important paper on stress concentration was published as early as 1898 by G. Kirsch [5]. He investigated the stress distribution around a small circular hole in a wide plate subjected to uniform longitudinal tension and showed that the localized stress occurring at the boundary of the hole (at the ends of the diameter perpendicular to the direction of the applied stress) was three times larger than the applied stress.

The tests carried out by Coker [6, 7] represented a valuable pioneering attack on the problem of stress concentration by photoelastic stress analysis. However, the accuracy of Coker's results was not too great owing to the use of compensation method at the edge of the hole or notch, a point of localized stress, where compensation method is particularly difficult to use. Tests by Preuss [8] using an extensometer were again not as accurate as might be desired because of the finite gauge length required and because of the lack of sensitivity in extensometers of short gauge length. The case of a circular hole near the straight boundary of a semi-infinite plate under tension parallel to the boundary was analyzed by Jeffery [9] and Mindlin [10] separately. Howland [11] discussed the case of a plate of finite width under tension with a circular hole on the axis of symmetry. Frocht [12] carried out studies in stress concentration (at the Carnegie Institute of Technology) by using the two-dimensional photoelastic methods in the mid nineteen thirties.

He found the factors of stress concentration in a variety of practical cases such as those of holes, grooves and fillets under the loading conditions of tension, compression and bending. He used the fringe value method on the photoelastic material, Bakelite BT - 61 - 893. Factors of stress concentration have been presented in the form of parametric curves and experiments showed that stress concentrations depend not only on the shape and dimensions of the discontinuity but also on the stress distribution on both sides of the discontinuity. It has been found that stress concentration factors are affected by any change in the dimensions of the body or in the method of supporting it which alters the stress distribution in one or both sides of the discontinuity.

Wahl and Beauwkes [13] studied holes and semi-circular notches in flat bars loaded under tension. A more accurate extrapolation method was employed in connection with fringe photographs obtained from photoelastic tests. Strain measurements on a large steel specimen having a hole, using Huggenberger extensometer were another means to determine the effects of stress concentration more accurately. Stress concentration factors determined were in general, found to be higher than those obtained by other investigators such as Coker [6,7] and Preuss [8]. However, the tests agreed closely with the mathematical results obtained by Howland [11] on bars with holes.

Because of the high stress concentration found at the edges of the hole, it is often necessary to reduce the stress concentration at holes, such as located in ship decks, airplane wings and fuselages.

In the case of a circular hole the effect of the reinforcement at the edge of the hole is to cause reduction in stress concentration. Timoshenko [14,15] observed the reduction of stress concentration etc., when a bead or a reinforcing ring is added in a flat tension member. He calculated the maximum stresses by using curved beam theory. Sazuki [16] reinforced the circular hole in a flat plate of epoxy resin with a ring of acrylic resin. He varied the axial thickness h of the ring in a specimen of constant thickness t and secondly he varied the inner radius R_1. The outer radius R_2 of the ring was the same as that of hole in the plate (Figure 2.1). It was found that the stress concentration factor (SCF) reduced remarkably with the increase of ratio $\frac{h}{t}$ up to 6 where it becomes more or less constant. Also SCF reduced with decrease of ratio $\frac{R_1}{R_2}$. SCF is quite small when $\frac{R_1}{R_2}$ is about 0.8.

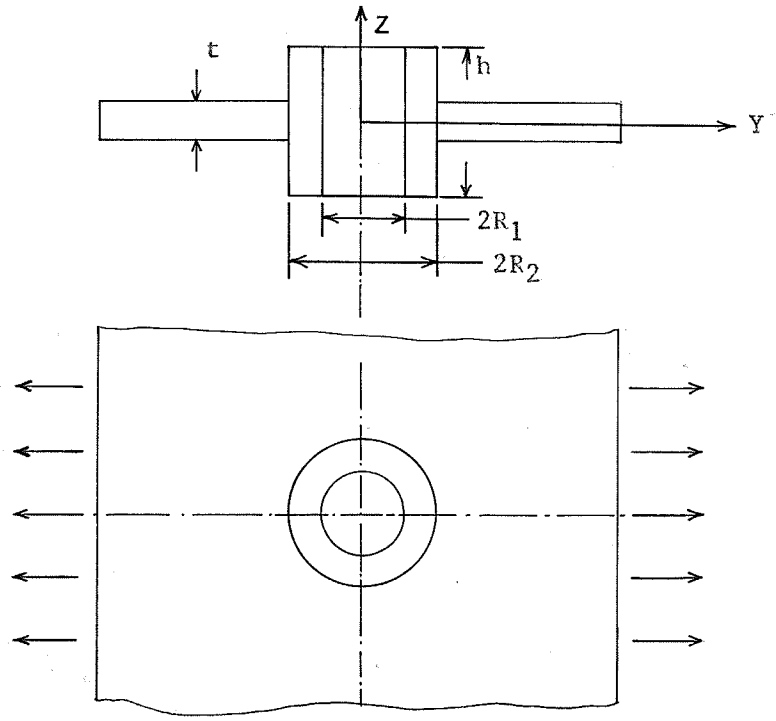

Figure 2.1 Ring of Acrylic Resin glued to Epoxy Resin Plate.

Other works concern the stress concentration at two or more holes, variously arranged in infinite plates [17, 18, 19, 20, 21, 22] and the corresponding problems in strips of finite width [23, 24]. Connected with the solutions about stress concentration at many holes is the study of superposition and interaction effects, which means the stress relief or reduction of stress concentration due to the presence of more than one discontinuity.

Notches in flat pieces and cylindrical grooves in round bars have an effect similar to that of holes. The stress concentration at notches of various shapes was investigated in a great number of research works. Neuber [25] dealt with the problem of grooves and notches by mathematical analysis and his results of the values of theoretical stress concentration factor at root of notch are available in the form of Neuber's diagram (nomograph) [26, 27].

Babuska and Kautsky [28] investigated the optimal forms of notches and fillets under tension and shear and thus determined the notch shapes leading to the lowest maximum stresses. The influence of the notch angle on the stress concentration factor was studied by Hahn [29]. Solutions for strips of finite width with semi-circular notches under tension were, for the first time given by Ling [30]. It was, however, pointed out by Peterson [31] and Frocht [32] by comparison with their accurate photoelastic measurements that Ling's results may be unreliable. So his results were improved by Isida [33], using a perturbation method, and by Atsumi [34]. The stress distribution at the contour of a notch in a plate under tension was examined in a preliminary

manner by Coker [35] using photoelastic method. By the photoelastic method, all types of plane stress concentration problems may be investigated. This was done extensively in the case of flat bars with fillets and double sided notches of various depths under tension and bending by Brown [36] and Frocht [32, 37, 38, 39].

The occurrence of high stresses around the contour of a notch has caused investigators to look into the possible means of reduction of stress concentration. Shimada [40], for instance, performed experiments using photoelastic principles to determine the effect of reinforcement on the stress distribution outside a semi-circular notch in bending. He pointed out that a most suitable selection of the reinforcement can help to reduce stress concentration so as to approach the values of bars without the semi-circular notch. Murakami and Kawabe [41] studied the effect of double notches on flat bars, in such a way that a second notch was made at the root of the first notch. They concluded that the stress concentration factor for a double notch is less than the product of independent SCF of each notch but greater than the SCF of individual notches independently.

It is also known that, by additional notches or holes in the vicinity of a single notch, the degree of stress concentration is lowered. One theoretical treatment of such effects was done by Nishihara and Fuji [42], who also conducted fatigue tests of single and multiple-notched bars. It was recognized as early as 1931 by Thum and Berg [43] that there always results a considerably higher fatigue strength for the parts with additional notches. Also, Okubo [44] dealt with this problem.

Photoelastic investigations of the effect of multiple notches were done by Durelli and others [45]. Nishioka and Hisamitsu [46] studied the influence of notch depth in the bending of flat plates of finite width in connection with the multiple notch effect. They also performed photoelastic tests.

The fact that, by additional notches, some stress relief, namely, a decrease of the stress concentration, as well as an increase of the stress concentration can occur has been known for some time, a consideration of such effects being given by Thum and Svenson [47, 48]. When three-dimensional notches or holes are penetrating each other, there may occur also a considerable increase of the stress concentration and for some of these cases, Thum and Svenson gave an approximate method for the determination of the SCFs.

In a paper by Paul and Faucett [49], it is indicated that the stress concentration factor of combined notches may be calculated in a simple way from the SCFs of the single notches, but this is no generally valid procedure and may be applied only in the cases when one stress raising notch is placed in the region of the maximum influence of a second notch. It was pointed out that the resulting SCF is then the product of the SCFs of the single notches.

A paper published out of a doctoral thesis by Vicentini [50] signifies the effect of superposition of notches on SCFs. For a strip with two notches of different radii, it may be seen that:

(a) When the two notches are far from each other, the SCF in each of the notch sections is practically unaffected by the geometrical parameters

of the other notch.

(b) When the two notches are closer together, the maximum stress depends both on geometrical parameters of the notches and the mutual spacing. In general, the resulting SCF is lower than the single SCF calculated for a strip with a single notch on each edge.

(c) When the notches are so close as to become superposed such that there is a presence of a second smaller notch in the root of a larger notch then the SCF due to a single larger notch is increased.

Also the resulting SCF is lower than the product of the two single SCFs, and as the ratio of the radii of smaller notch to that of larger notch decreases, the SCF tends to be still lower. When either the depth of the smaller notch is great or the ratio of radii of smaller to larger notch approaches unity, the resulting SCF tends, on the contrary to that of a smaller notch.

Apart from this, few other suggestions for reducing the stress concentration are mentioned in the references such as [26, 51, 52, 53, 54, 55, 56].

The investigations of the authors previously referred to are useful. However, the problem of investigation constituting the reduction of stress concentration to a certain optimum stage, at the edge of a circular hole or root of V-notch by removal of material in a specific manner,

in the neighbourhood of stress raiser, has not been dealt with and thus urged the author to embark upon the experimental research programme described in this thesis.

CHAPTER 3

FUNDAMENTAL PRINCIPLES OF STRESS CONCENTRATION

3.1 Introduction

The theoretical principles involved in reduction and evaluation of stress concentration effects supported by experimental work are discussed in this chapter.

3.2 Reduction of Stress Concentration

It is known that the stress concentration reduces the fatigue strength of a loaded member. So the question arises, why not reduce the stress concentration so that an improved fatigue strength may be achieved? Some of the methods that have been employed in an attempt to partly overcome the damaging effects of localized stresses are indicated in references such as [26, 51, 56]. One method of reduction of stress concentration is by material removal. This method can be explained by the streamline analogy.

3.3 Streamline Analogy

From the design point of view, the effects of stress concentration and its possible reduction by material removal can best be understood by applying the streamline analogy, for instance, to a flat plate with edge notches as shown in Figures 3.1a, b.

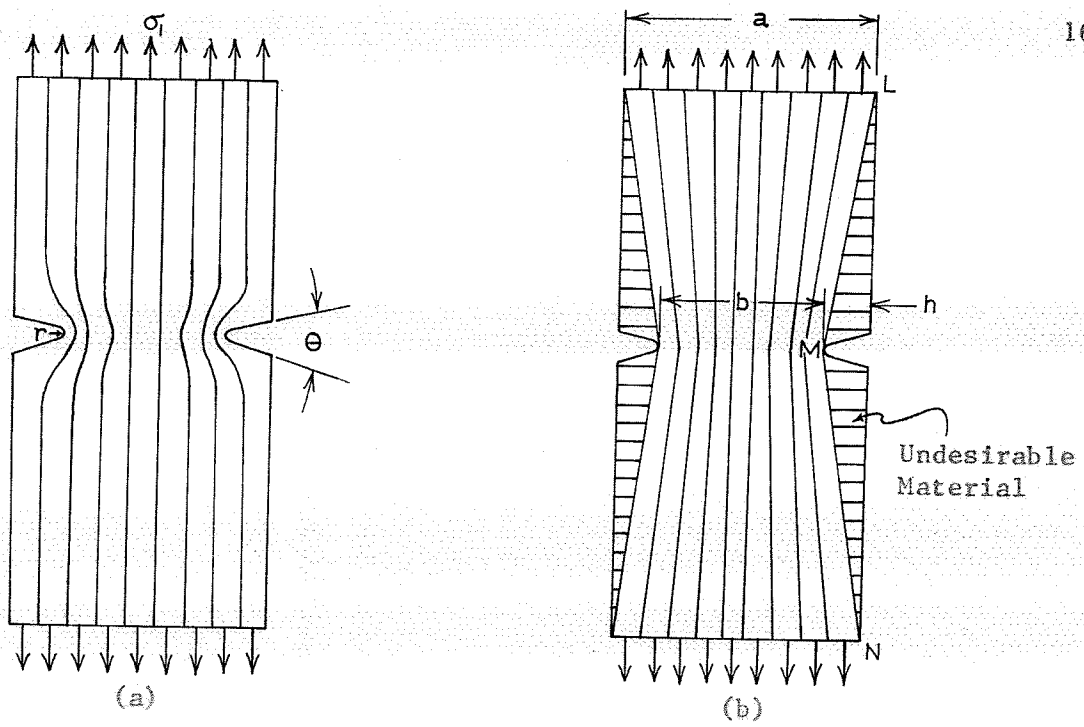

Figure 3.1 Stress Concentration Analysis in V-Notches by Lines of Constant Force (Forcelines).

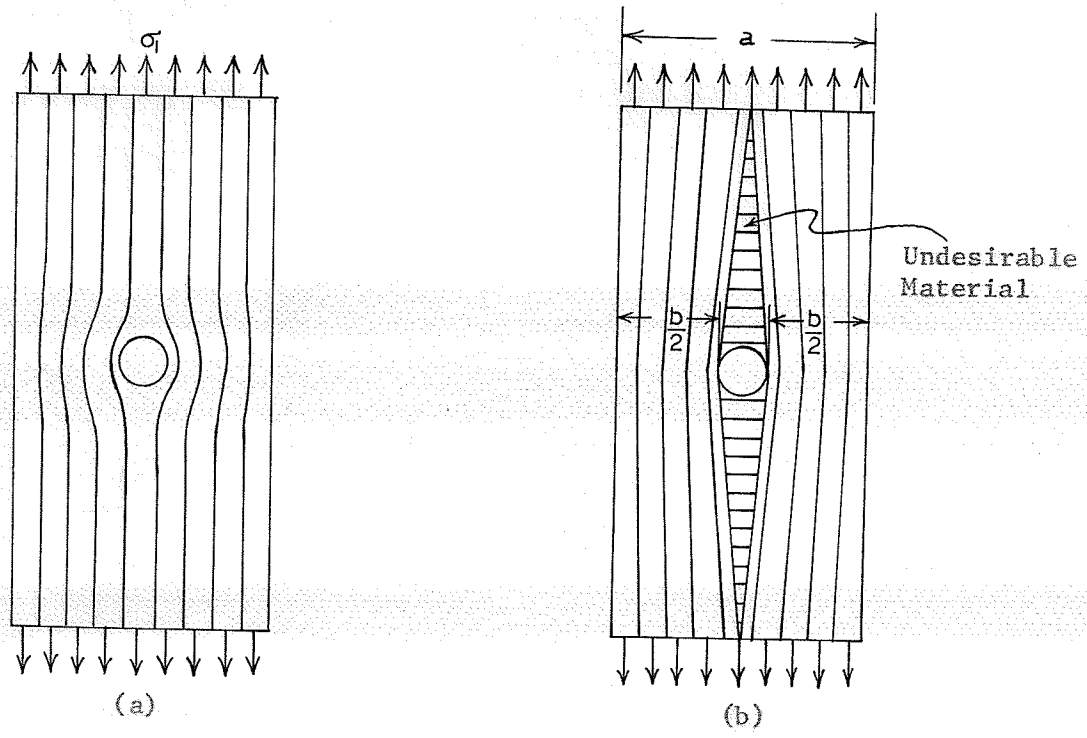

Figure 3.2 Stress Concentration Analysis in a Circular Hole by Lines of Constant Force (Forcelines).

A uniformly distributed force σ_1 per unit length is applied at the ends, which are some distance away from the notches. The width 'a' can be arbitrarily divided into a number of equal segments Δa, so that each of these segments is acted upon by the same force ΔP. In the same way, the width 'b' can be divided into the same number of elements of width Δb on the assumption that a uniform stress distribution is desired over the material between the two notches. This is shown in Figure 3.1b. Each of the elements Δb is acted upon by the same force ΔP again, such that the value of σ will be increased in the ratio $\frac{a}{b}$, but will be constant over the section. The nominal stress is, of course, equal to $\frac{\sigma_2}{t}$ and is also uniformly distributed. Now the corresponding elements can be connected by means of straight lines as shown. Such lines can be thought of as force lines in the present explanation, though these are referred to as streamlines in fluid dynamics. The force lines represent the paths over which the force being transmitted is constant. Also, there will be very little change in the direction of these lines in the notched region, if the ends of the plate are sufficiently far removed from the notches. Therefore, it can be concluded that the effect of stress concentration would be negligible if the plate conforms to the shape formed by the force lines. In Figure 3.1b, the actual plate has been shown to include the extra material in the shaded portions LMN, designated as "undesirable". This reveals the proper way to eliminate or reduce the effects of stress concentration.

This method of analysis thus stimulates the idea of stress concentration reduction and explains why it is possible to relieve stress concentration, the object obviously being to remove or weaken the undesirable material.

This analogy may be equally well applied in the case of a hole in a plate as illustrated in Figures 3.2a,b. This analysis also indicates, in a general way, the effects of the variables that control the shape of the notch and hole. The magnitude of the additional force flow is controlled primarily by the diameter in case of hole and the notch depth (Figure 3.1b). The notch angle θ has the effect of removing undesirable material as θ increases. Obviously, when θ is very large, the ideal situation of removing all of the undesirable material can be approached, thus eliminating the stress concentration or reducing it to the minimum. The notch radius determines the intensity of the stress over a very small area at the root of the notch.

In the present context of the problem, the removal of material in the neighbourhood of the'stress raiser'has been resolved by the introduction of varying sizes of 'stress reducers' arranged symmetrically beside the raiser, in keeping with the principles of streamline analogy. The geometrical shape of reducer is similar to that of raiser. In a way it may be said to be analogous to the interference or superposition effect of like discontinuities.

3.4 Evaluation of Stress Concentration Factor

The stress concentration factor for a given discontinuity is defined as the ratio of the maximum (localized) stress to the nominal stress. The nominal stress can be calculated depending on the size of the discontinuity relative to the area in which it is existing. For example, in a plane stress case for a wide flat plate under uniaxial tensile load P, and containing a relatively small hole, the nominal stress σ_{nom} can be calculated as

$$\sigma_{nom} = \frac{P}{A_g}$$

Where A_g = Gross area, including the area removed at the hole.
But if the size of the hole is relatively large or other abrupt changes in section occur in which there is a considerable reduction of area in a member caused by the stress raiser, the nominal stress is usually calculated on the basis of net area.

$$\sigma_{nom} = \frac{P}{A}$$ where A = net or minimum cross sectional area.

The stress concentration factor can be classified in two ways. One is known as the 'theoretical (elastic) stress concentration factor', K_t, and the other as 'effective or significant stress concentration factor', K_e. K_e is the value found from the tests of the actual material under the conditions of use, as for example, under repeated stress by the

determination of the endurance limit, first from specimens containing a hole or notch or any abrupt change in section, and then obtaining the endurance limit from specimens free from any such discontinuity. K_e, when calculated in connection with repeated loads (fatigue) may be also termed as fatigue strength reduction factor, K_f.

If σ_{max} in a member is the theoretical value of the localized stress as found with the help of the mathematical theory of elasticity, or the photoelasticity method, then it is called the theoretical stress concentration factor denoted by K_t. In mathematical form,

$$K_t = \frac{\sigma_{max}}{\sigma_{nom}} = \frac{\sigma_{max}}{P/A} \qquad (3\text{-}1)$$

3.5 Determination of K_t from Photoelastic Data

Two photoelasticity techniques can be used in the determination of maximum stress or the stress concentration factor. These are Photographic Method and Fringe Value Method. Both were employed by Frocht [12, 37] in his photoelastic studies on stress concentrations. These methods directly depend on the basic stress optic law of photoelasticity in two dimensions.

Stress Optic Law in Two Dimensions

The law states that in a transparent, homogeneous, isotropic material having the property of birefringence, when subjected to stress within the elastic limit, the retardation in wavelengths between the

two perpendicular light components travelling through the material at a point is linearly proportional to

1. the difference of the principal stresses lying in the plane perpendicular to the axis of propagation;
2. the thickness of the material in the direction of the axis of the propagation;
3. inversely proportional to the wavelength of light passing through the material.

In the mathematical form, the law can be written as

$$\Delta = \frac{2\pi hc}{\lambda} (\sigma_1 - \sigma_2) \quad * \qquad (3\text{-}2)$$

where Δ = Relative retardation

c = Realtive stress optic co-efficient and expressed in terms of Brewsters (1 Brewster = 10^{-3} cm^2/dyne).

h = Thickness of the model material in inch.

$\sigma_1 - \sigma_2$ = Principal stress difference.

Since the units associated with the Brewster are not commonly employed in engineering practice, equation 3-2 may be conveniently written in a

---

* This is a standard accepted law derived on the property of birefringence of any photoelastic material. Its derivation is available in any reference or text book dealing with the principles of Photoelasticity e.g., References [52, 61, 62].

modified form as given below

$$\sigma_1 - \sigma_2 = \frac{Nf_\sigma}{h} = NF \qquad (3\text{-}3)$$

where $N = \frac{\Delta}{2\pi}$ = Relative retardation in a complete cycle of retardation, 2π.

N is a dimensionless quantity and is usually called the fringe order. It is different at some points of the model in study and is actually the physical function of the polariscope to determine it.

$F = \frac{f_\sigma}{h}$ = Model fringe value, psi/fringe

$f_\sigma = \frac{\lambda}{c}$ = Material fringe value, psi-in/fringe.

The value of f_σ is established by means of calibration of a particular photoelastic material employed for experimental study.

Therefore, the stress optic law given by equation 3-3 can be used for the calculation of K_t at the point of maximum stress around the boundary of the discontinuity in a loaded member.

The normal principal stress is zero at the point of stress concentration on the boundary, and the tangential stress (tensile) to the boundary is then directly given by relation 3-3.

e.g., If $\sigma_2 = 0$

then $\sigma_1 = \frac{Nf_\sigma}{h}$ (3-4)

which indicates that for a photoelastic stressed model, f_σ and h being

constant for a particular material, the maximum stress at a point on the boundary is directly a function of maximum fringe order at that point.

$$\text{i.e.,} \quad \sigma_{max} = \frac{N_{max} f_{\sigma}}{h} \tag{3-5}$$

Fringe Value Method

This method requires knowledge of the maximum fringe order at the discontinuity and the applied load.

$$K_t = \frac{\sigma_{max}}{\sigma_{nom}} = \frac{N_{max} f_{\sigma/h}}{P/A} \tag{3-6}$$

Since equation 3-6 contains the fringe value f_{σ}, the method based on equation 3-6 will be referred to as the Fringe Value Method.

Photographic Method

This method is based on the auto-calibration and does not require knowledge of the material fringe value or the applied load, for determining K_t. The photographic method rests on the assumption that the stresses some distance from the discontinuity are uniform and that they can be accurately determined photoelastically. That is, the model must have a shank of uniformly distributed uniaxial stress where fringe order N_{nom} may be measured with respect to any point of zero fringe order.

Then the basic relation in this method is

$$K_t = \frac{\sigma_{max}}{\sigma_{nom}} = \frac{N_{max}\, f_\sigma/_h}{N_{nom}\, f_\sigma/_h}$$

$$K_t = \frac{N_{max}}{N_{nom}} \qquad (3\text{-}7)$$

In the two methods stated, the maximum fringe order can be determined either by extrapolation or by precise compensation at the point of interest at the boundary.

However, the determination of N_{nom} requires the use of a Babinet compensator. Also, another complication arising from the fact that generally no true uniform tension could be developed gives the belief that the accuracy of this method may not be as good as that of the fringe value method and thus restricts the use of the photographic method.

3.6 Magnitude and Position of Stress Concentration on the Boundary of the Discontinuity

(a) Circular Hole in a Uniaxial Tension Member

The stress distribution around a small circular hole in a thin flat plate of infinite dimensions subjected to a uniform tensile stress as shown in Figure 3.3 has been known from the mathematical theory of elasticity. The normal and shear stress components [11, 26, 27, 59] at any point e.g., point M whose coordinates are r and θ as in Figure 3.3 are given by the following expressions:

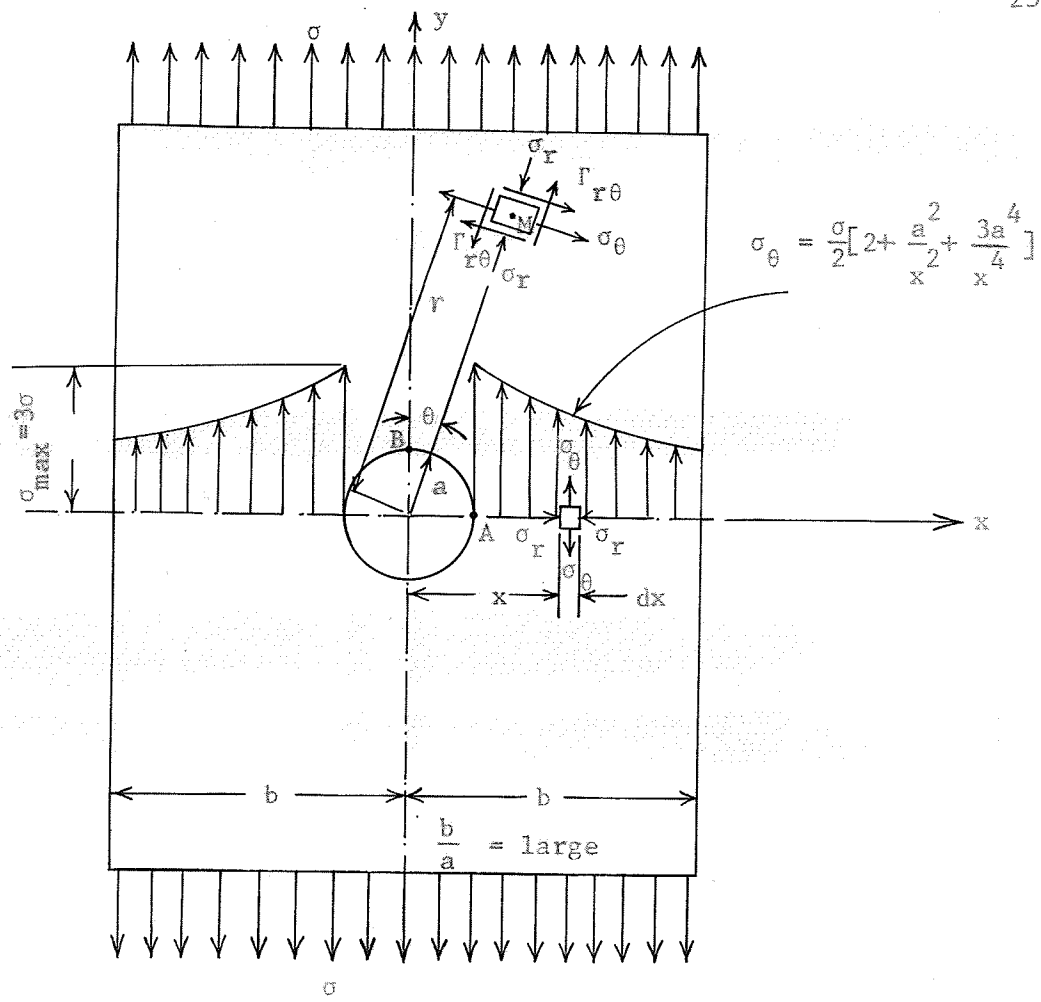

Figure 3.3 Stress Distribution in a Thin Plate Containing a Small Circular Hole.

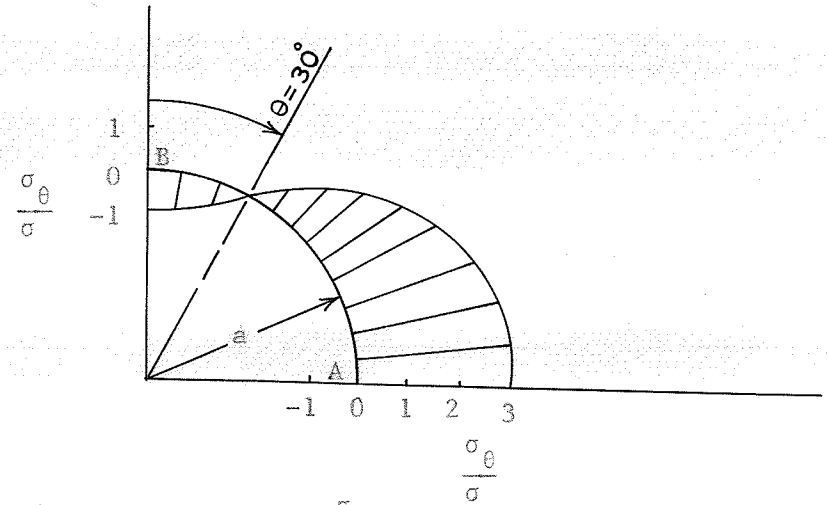

Figure 3.4 Distribution of $\frac{\sigma_\theta}{\sigma}$ around the Boundary of Hole.

$$\text{Radial stress} = \sigma_r = \frac{\sigma}{2}\left(1 - \frac{a^2}{r^2}\right) + \frac{\sigma}{2}\left(1 + \frac{3a^4}{r^4} - \frac{4a^2}{r^2}\right)\cos 2\theta \qquad (3\text{-}8)$$

$$\text{Tangential Stress} = \sigma_\theta = \frac{\sigma}{2}\left(1 + \frac{a^2}{r^2}\right) - \frac{\sigma}{2}\left(1 + \frac{3a^4}{r^4}\right)\cos 2\theta \qquad (3\text{-}9)$$

(Normal stress in a direction perpendicular to the radius)

$$\text{Shear stress} = \Gamma_{r\theta} = -\frac{\sigma}{2}\left(1 - \frac{3a^4}{r^4} + \frac{2a^2}{r^2}\right)\sin 2\theta \qquad (3\text{-}10)$$

where σ = uniform tensile stress at the ends of the plate and also the stress that would exist at the point, if the plate had no hole. To see the stress distribution at any point on the section through A, and at a distance x from the centre of the hole, $\theta = 90°$ and $r = x$, equations 3-8 and 3-9 reduce to

$\sigma_r = 0$ This being particularly at the point when $x = a$

$$\text{and } \sigma_\theta = \frac{\sigma}{2}\left[2 + \frac{a^2}{x^2} + \frac{3a^4}{x^4}\right] \qquad (3\text{-}11)$$

The distribution of σ_θ given by equation 3-11 on the section through A, is as shown in Figure 3.3. σ_θ rapidly approaches σ as x increases and follows the radius outwards from A. At the edge of the hole i.e., at

$\theta = 90°$, $x = a$,

$$\sigma_\theta = \sigma_{max} = 3\sigma \qquad (3\text{-}12)$$

$$\text{or } \frac{\sigma_\theta}{\sigma} = 3 = SCF \qquad (3\text{-}13)$$

Equation 3-13 states that the stress at the edge of a small hole in an infinitely wide plate subjected to a uniform tensile stress in one direction is three times the value of the uniform stress that would occur at the same point if there were no hole in the plate.

Similarly, at point B as shown in Figure 3.3 the stress may again be found by substituting $\theta = 0°$ and $r = a$ in equation 3-9.

$$\sigma_r = 0$$
$$\text{and} \quad \sigma_\theta = -\sigma \tag{3-14}$$

$$\text{or} \quad \frac{\sigma_\theta}{\sigma} = -1 = SCF \tag{3-15}$$

equation 3-14 states that the tangential stress σ_θ becomes compressive and of magnitude equal to the uniform tensile stress acting in the plate. Equations 3-13 and 3-15 give the values of theoretical stress concentration factor at the points A and B respectively, showing thereby that the stress concentration is more dominant at the position of the point A than at the point B on the edge of the hole. The distribution of stress around the boundary of the hole is obtained by setting $r = a$, into the equations 3-8, 3-9 and 3-10.

$$\sigma_r = \Gamma_{r\theta} = 0$$
$$\sigma_\theta = \sigma(1 - 2\cos 2\theta) \tag{3-16}$$

$$\text{or stress concentration factor} = \frac{\sigma_\theta}{\sigma} = 1-2\cos 2\theta \tag{3-17}$$

The distribution of $\frac{\sigma_\theta}{\sigma}$ around the boundary of the hole, as described by equation 3-17 for the various values of angle θ is as shown in Figure 3.4. At the point defined by $\theta = 30°$ on the boundary of the hole, $\frac{\sigma_\theta}{\sigma} = 0$ i.e., all stresses become zero. Such a point is commonly referred to as a singular point. Howland [11] modified this mathematical analysis to

be applied without much error to plates of finite width which are quite a common occurrence in the engineering practice. As the plate becomes narrower, the value of stress concentration factor drops off as indicated by Figure 3.5 obtained from reference [51]. For a single hole of 5/16" diameter acting as a stress raiser in a shank width of 1 inch and thickness 1/4", of a tension model, the value of stress concentration factor, K_t, as given by the curve in Figure 3.5 is 2.3. The use of reducers to lower the value of K_t still further below the value found, will be observed in the experimental study.

(b) Symmetrical V-Notches in Uniaxial Tension Member

The stress distribution at a section through the root of symmetrical V-notches as obtained by Coker [35] with the photoelastic method is shown in Figure 3.6. Also, the stress distribution along different radii of root at the contour of either V-shaped notch is illustrated by magnitude profile in Figure 3.7 with radial lines indicating the magnitude of stress. These two figures obviously depict that the maximum stress occurs at the root of the notch and at a point B on the contour where the radius is perpendicular to the direction of load. Any value of K_t, from 1.0 to infinity, can theoretically be obtained by notches of varying geometry, the value approaching infinity as the ratio of notch radius to depth approaches zero. However, the theory is modified by Neuber [25] for small root radii. The magnitude of K_t for various ratios of notch root radius to depth are available in reference [64].

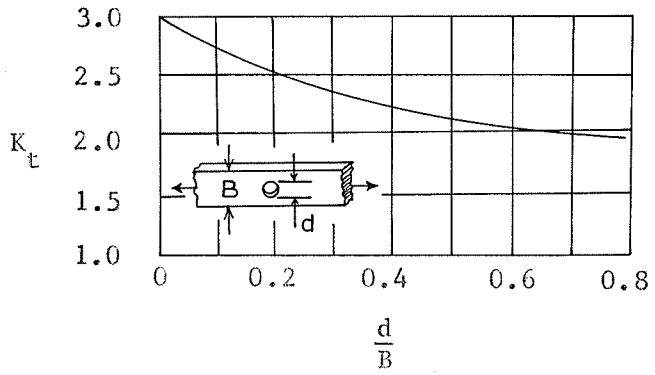

Figure 3.5 Stress Concentration Factor for a Flat Plate with Central Hole in Tension.

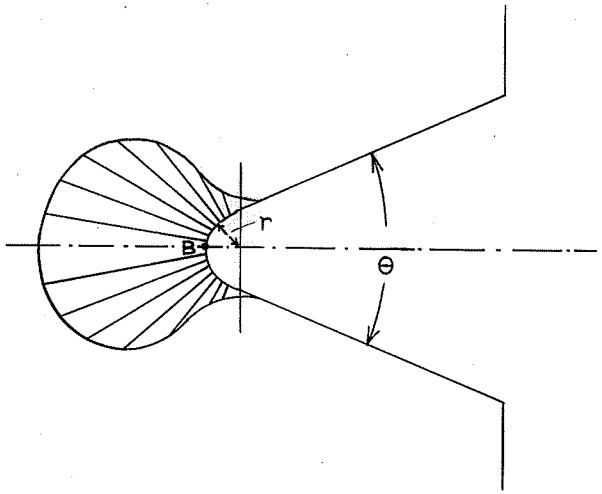

Figure 3.7 Magnitude Profile of Stress Distribution at the Contour of a V-Notch.

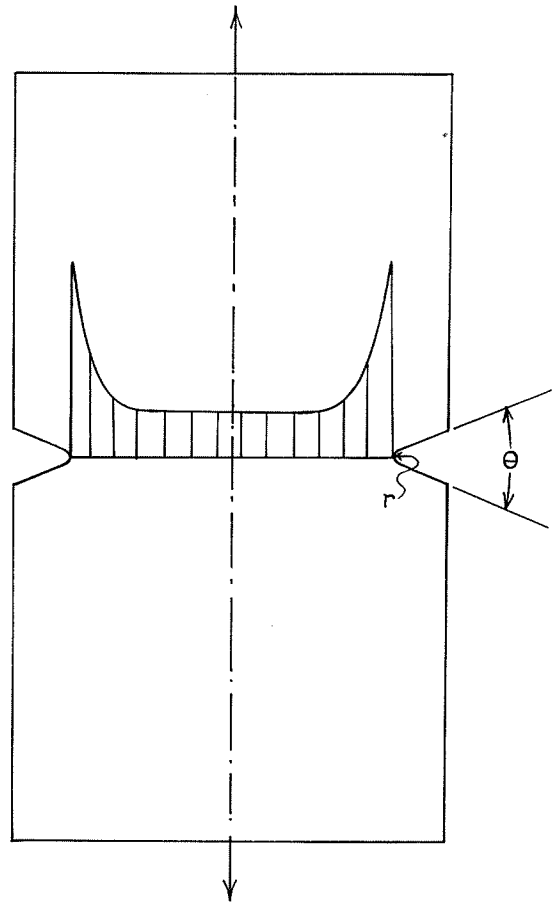

Figure 3.6 Stress Distribution at Section of a V-Notch.

CHAPTER 4

EXPERIMENTAL STUDY

4.1 Introduction

As noted in Chapter 2, most of the research on stress concentrations was in plane stress study, carried out to investigate the effect of holes, notches and other discontinuities. Reduction of stress concentration by 'material removal' is already known. In the present experimental study, a new approach in the way of material removal has been taken. The study was on models loaded in tension, and conducted in the Photoelasticity Laboratory of the Faculty of Engineering of The University of Manitoba.

There are various experimental methods existing in practice for studying the effects of stress concentration. Photoelastic stress analysis is one of the most powerful experimental techniques and was, therefore, chosen for the investigation.

4.2 Photoelastic Model Materials

The selection of the proper materials for a photoelastic model is one of the most important factors entering into photoelastic stress analysis. A perfectly ideal photoelastic material does not exist. However, a good type should exhibit the necessary properties such as transparency and birefringence, high sensitivity (low material

fringe value), high elastic limit, good machineability, low optical and mechanical creep, low time edge effects, freedom from residual stresses, high Young's modulus and a high ultimate strength. The ratio of Young's modulus and material fringe value is known as the 'figure of merit' of the material. A high figure of merit is preferable.

Epoxies are the most recent additions to the class of materials used for the manufacture of photoelastic models. Epoxy resin mainly finds its application in three-dimensional study, but its properties of high sensitivity, low optical creep and time edge effects favour it for two-dimensional work as well. It is available commercially in the form of sheets. Also, epoxy is available as pure resin which has to be mixed with a hardener to be polymerized. An attempt was made in the photoelastic laboratory to cast small size sheets with liquid araldite (belongs to the family of epoxies), but the occurrence of residual stresses prohibited its direct use in the experimental study.

Therefore,a polyester (type of epoxy) sheet material, supplied under Type Number PSM - 1, by the manufacturers Photoelastic Incorporated,was selected. The manufacturers specifications of the material PSM - 1 are as shown in Table 4 - 1. The material fringe value or the stress optical constant was found by calibration as shown in Appendix B.

4.3 Specimen Details

The nominal specimen dimensions are shown in Figure 4.1. The load was applied through the brass bushings which increased the bearing area.

TABLE 4-1

MANUFACTURERS SPECIFICATIONS OF PHOTOELASTIC MATERIAL PSM-1 *

Type Number	Description	"f_σ" stress Optical Constant (psi/fringe/inch)	E (1000 psi)	μ Poisson's Ratio	Nominal Thickness	Standard Sizes
PSM-1	A clear polyester sheet, excellent for two-dimensional model work. Free of creep and edge effects, with highest photoelastic sensitivity of any known photoelastic model material available.	40	340	0.38	0.250	Standard sheets available from stock are 10"x 10" supplied with protective paper coating (both sides) for tracing model shape without scratching plastic.

* Supplier - Photoelastic Incorporated

67 - Lincoln Highway, Malvern, Pa., USA.

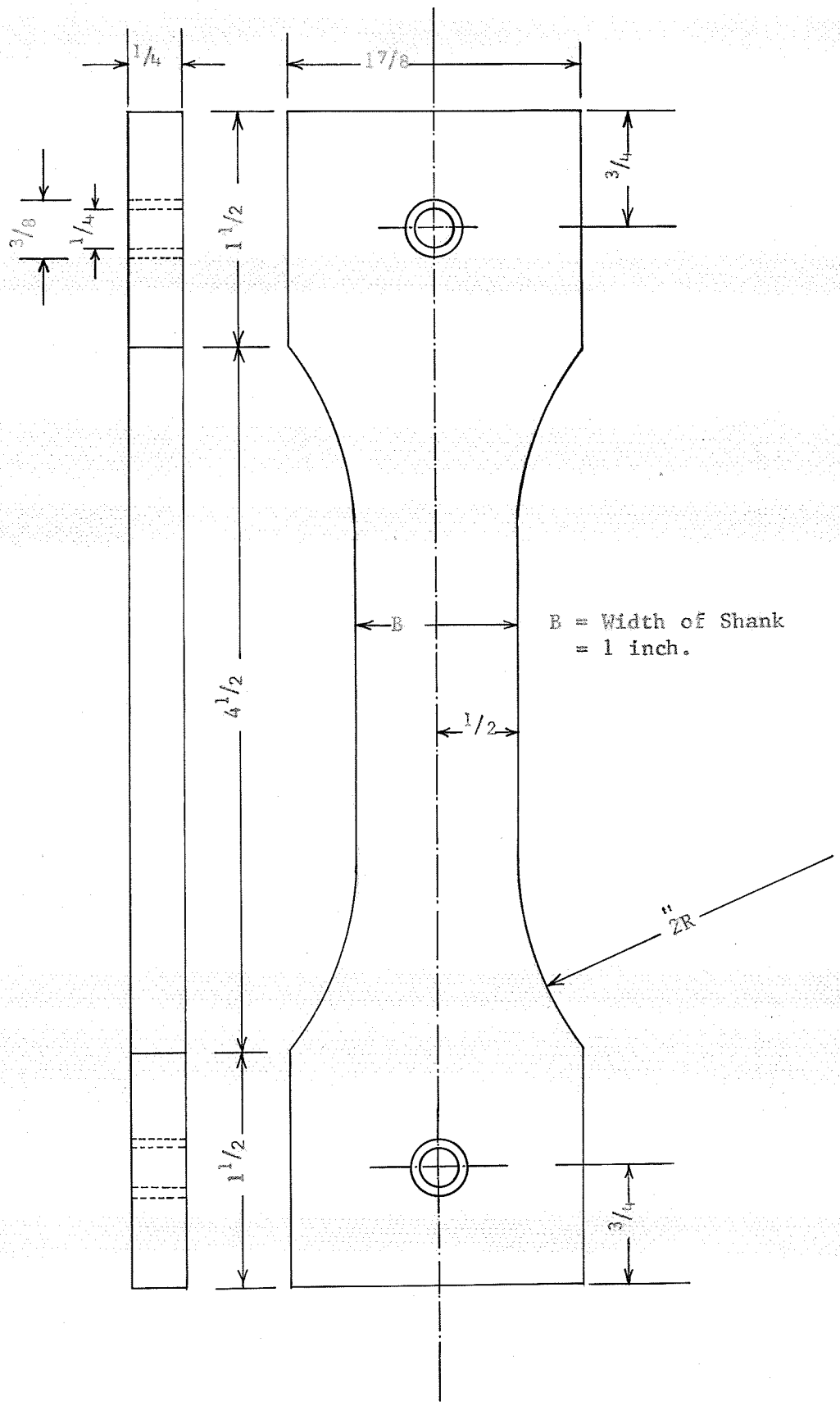

Figure 4.1 Tension Specimen Dimensions in inches.

The portions of the shank studied in the two series of specimens are shown in Figures 4.2 and 4.3. One type, H, employed a circular hole and the other, N , used double symmetrical V-notches as the stress raisers. Sixteen models were used in each series thus making a study of thirty-two models in all. Various models were designated by the addition of proper numeral subscripts to the letter H or N for their individual recognition, depending on the sequence of material removal. This can be seen in Table 4.2.

The basic idea of the experimental analysis was to investigate the possibility of reducing stress concentration effect by means of material removal in the neighbourhood of a stress raiser. The discontinuity introduced to create stress concentration has been named as stress raiser and the material removed in the neighbourhood of stress raiser, giving rise to new discontinuity has been called stress reducer. The said discontinuities have been named as such simply for the sake of convenience in their designation, though their effects are actually interdependent.

The stress raiser was located in the mid section of shank length in all models. The first models in H and N series contained only the stress raiser and are designated H_{10} and N_{10} respectively. The stress reducer consisted of a geometrical shape similar to that of stress raiser. As an illustration, the combined configurations of five models in each sub-series H_1 and N_1 separately can be seen in the respective Figures 4.2 and 4.3. The models in sub-series H_2, H_3 and

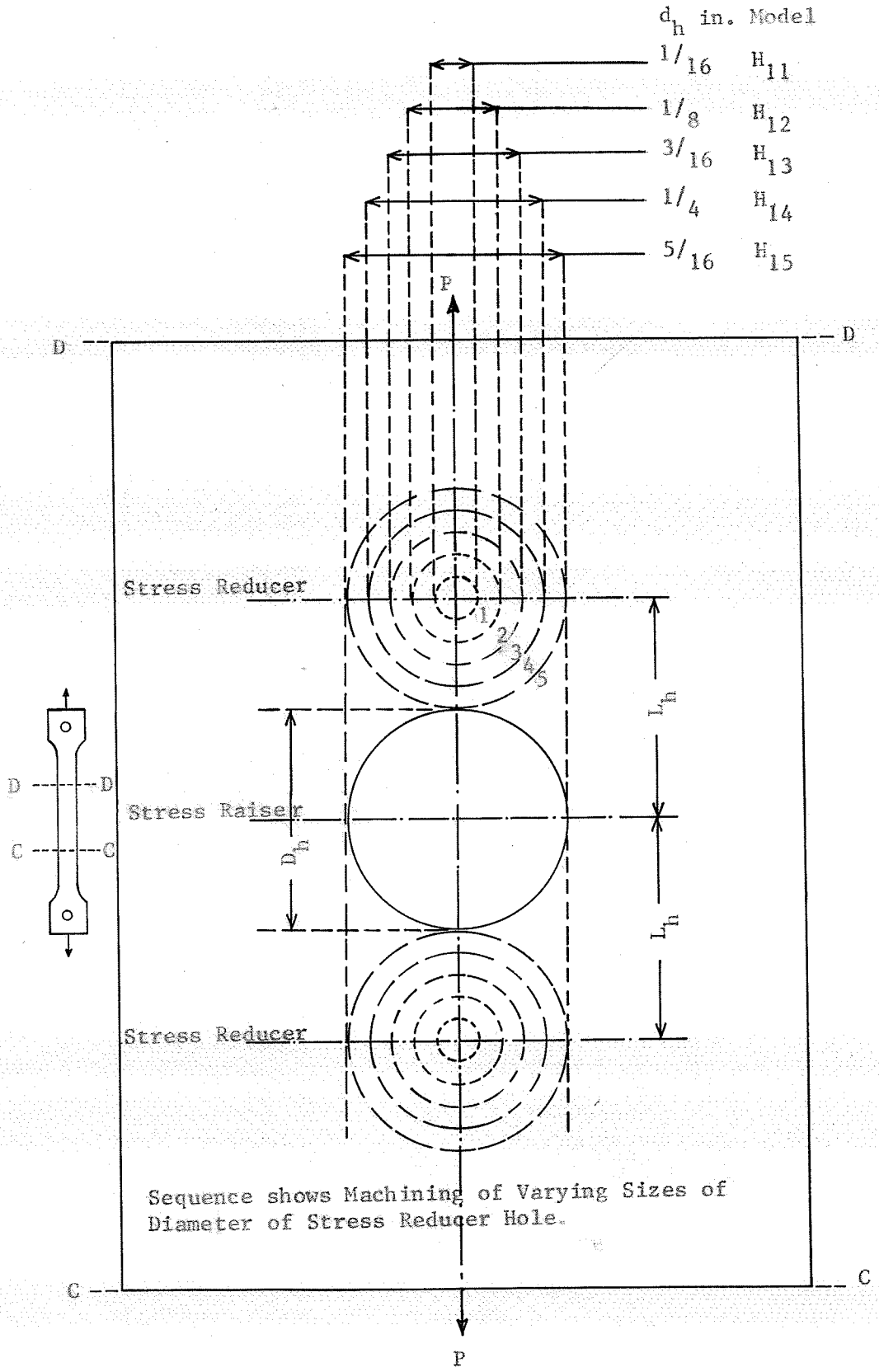

Figure 4.2 Portion of Shank of Specimen in Series H_1.

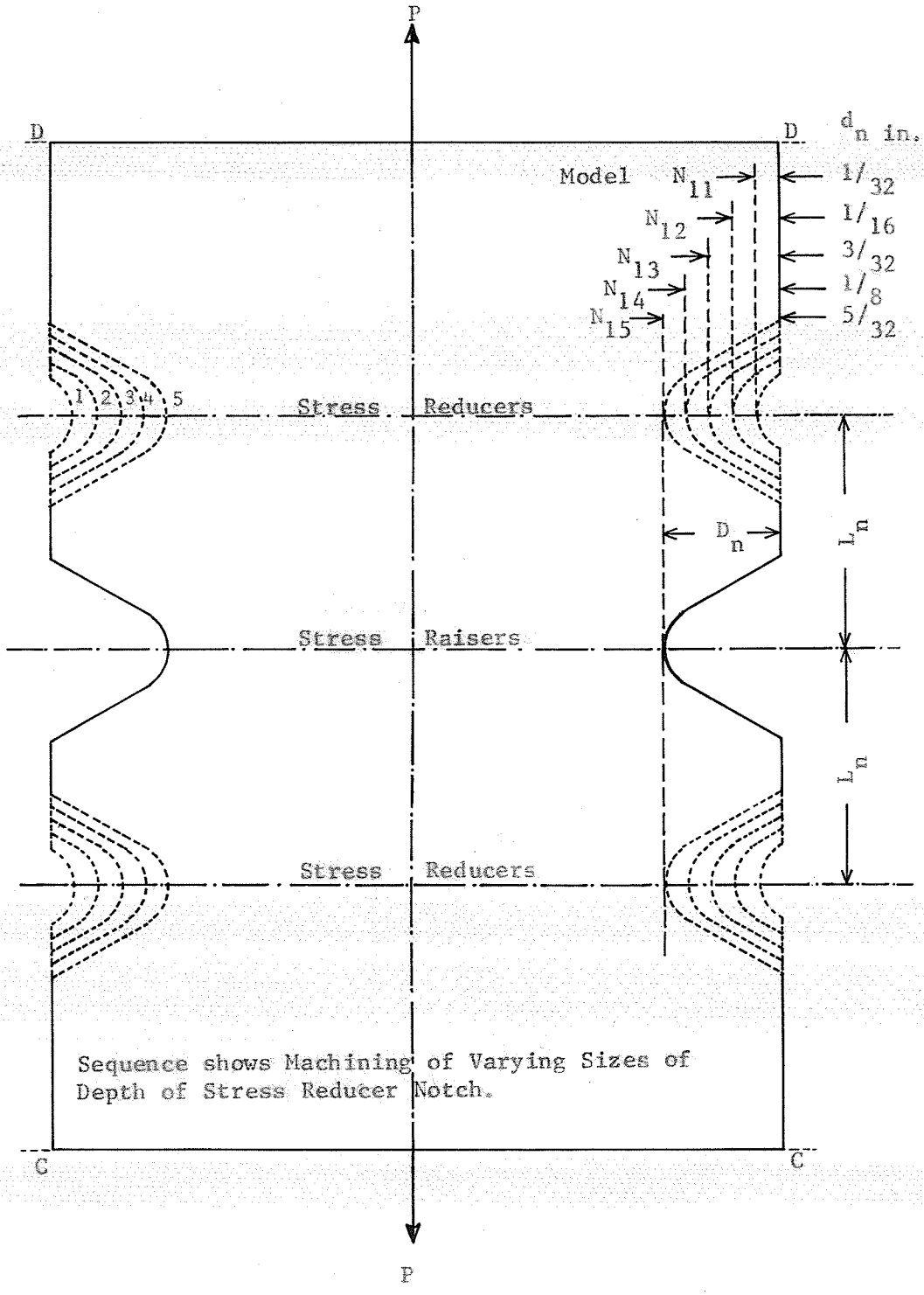

Figure 4.3 Portion of Shank of Specimen in Series N_1.

TABLE 4-2

NOMINAL DIMENSIONS OF THE

INDIVIDUAL MODELS

Nomenclature Refers to Figures 4.2 and 4.3

Series	Sub-series	D_h or D_n (in)	L_h or L_n (in)	$\frac{L_h}{D_h}$ or $\frac{L_n}{2D_n}$	Model Classified depending on the sequence of material removal or stage of variation of diameter or depth of stress reducer.					
H	H_1	5/16	5/16	1	Model	H_{11}	H_{12}	H_{13}	H_{14}	H_{15}
					d_h	1/16	1/8	3/16	1/4	5/16
	H_2	5/16	15/32	1.5	Model	H_{21}	H_{22}	H_{23}	H_{24}	H_{25}
					d_h	1/16	1/8	3/16	1/4	5/16
	H_3	5/16	5/8	2	Model	H_{31}	H_{32}	H_{33}	H_{34}	H_{35}
					d_h	1/16	1/8	3/16	1/4	5/16
N	N_1	5/32	5/16	1	Model	N_{11}	N_{12}	N_{13}	N_{14}	N_{15}
					d_n	1/32	1/16	3/32	1/8	5/32
	N_2	5/32	15/32	1.5	Model	N_{21}	N_{22}	N_{23}	N_{24}	N_{25}
					d_n	1/32	1/16	3/32	1/8	5/32
	N_3	5/32	5/8	2	Model	N_{31}	N_{32}	N_{33}	N_{34}	N_{35}
					d_n	1/32	1/16	3/32	1/8	5/32

Nomenclature

H - Series

D_h = Diameter of stress raiser (kept constant in all models)

d_h = Diameter of each stress reducer (varied in individual models depending on sequence of material removal)

L_h = Pitch of holesi.e., centre to centre spacing between raiser and each reducer

N - Series

D_n = Depth of each edge stress raiser (kept constant in all models)

d_n = Depth of each stress reducer (varied in individual models depending on sequence of material removal)

L_n = Pitch of notches i.e., root to root spacing between each raiser and reducer

Root radius was kept constant as 1/16" and same for raiser and reducer notch.

Some dimensional similarity was also maintained between holes and notches. For example

Radius of hole = Depth of corresponding notch.

and $L_h = L_n$.

N_2,N_3 were composed simply on the basis of different pitch than those of series H_1 and N_1.

4.4. Making of Models

In order to accommodate the study of 32 different models as mentioned earlier only six photoelastic specimens were prepared on the milling router, three for each series, H or N. Each model was re-used by enlarging the size of stress reducer in the order of sequence, thus resulting in the shape of different models in the individual sub-series H_1, H_2, H_3, N_1, N_2 and N_3. For making the particular model for study in H-series, a steel template 3/16 inch thick, manufactured to enclose the requisite size of stress raiser and stress reducers was used as a jig for drilling holes through model material. The point angle of each drill was ground approximately to 80 degrees to reduce machining stress on the boundary of holes. The V-notches were machined on the edges of the models in N-Series on a small shaper. The shaping tool was made of high speed steel with cutting edges ground to include a notch angle of approximate 60 degrees and a root radius of 1/16 inch. The particular model was sandwiched between two or more dummy models of similar or cheaper material and held in the vice on the shaper. With this sandwiching arrangement the shaping tool could not directly hit the edge of the actual model. This avoided chipping off at the notch edges and minimized the machining stresses as well. The root radius and angle of notch were kept unaltered throughout the experiment on notches.

Sufficient care was taken to make stress free models. However, it may be mentioned here that the sheet material PSM-1 supplied by the manufacturers contained some residual stresses and the blanks for the models were thus including these residual stresses. To avoid these initial stresses and also the machining stresses, annealing process was tried on one or two specimens with the annealing oven available in the laboratory. But for an automatic temperature control on the oven, the annealing process did not give favourable results. Therefore, the models were used, as they were, without any annealing. The coolant under air pressure was employed throughout the cutting operations of the models to keep the machining stresses to a minimum.

Figures 4.4, 4.5, and 4.6 show the milling router, drill, and shaper employed for necessary machining operations with the action of coolant jet.

4.5 Equipment

The main elements of the equipment used for the photoelastic experiment are:

1. A Circular Polariscope

Both diffused light type and lens type circular polariscopes are available in the laboratory, but the former was used because of its advantages [62] over the latter. The diffused light type polariscope used consists of 12 inch diameter elements (Polarizer, Analyzer, two quarter wave plates). The straining frame, which constitutes an integral part of the polariscope unit, is provided with a piston-cylinder

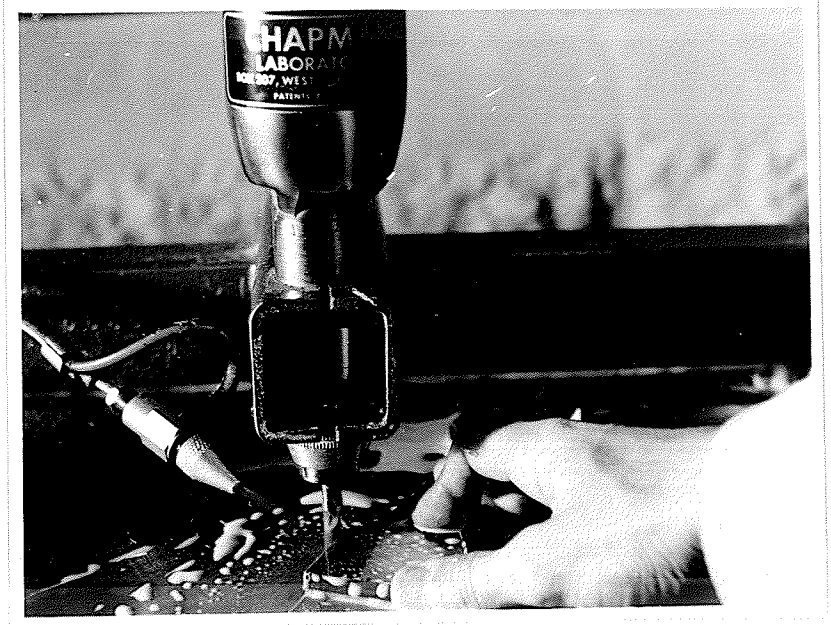

Figure 4.4 Milling Router Machining the Model Profile

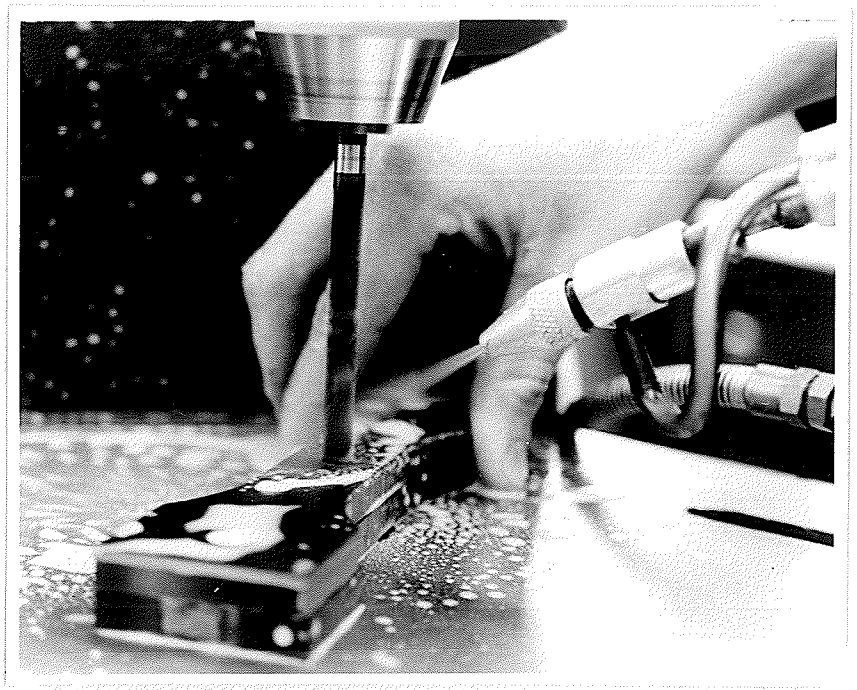

Figure 4.5 Drilling of Hole in the Model

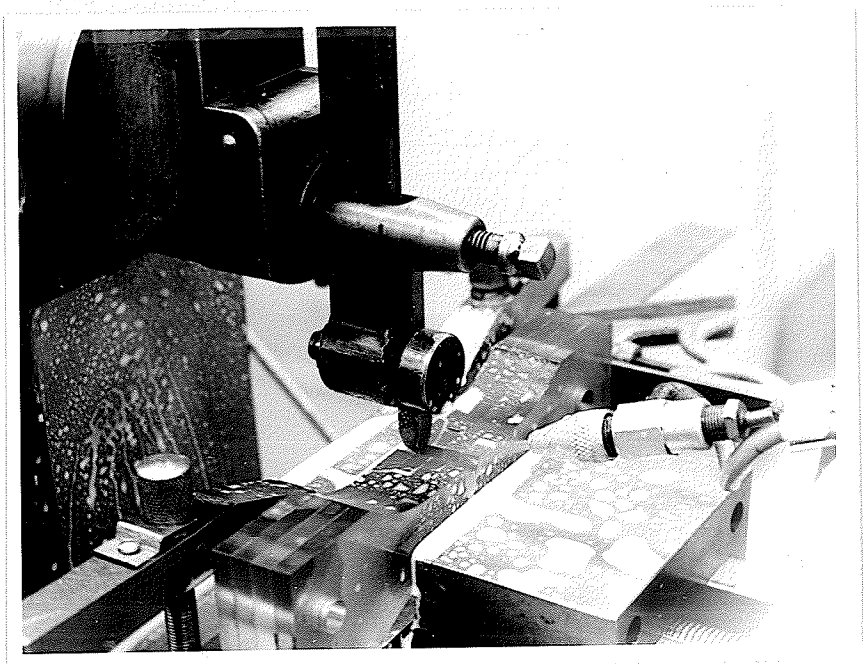

Figure 4.6 Shaping Tool Machining Edge V-Notch on the Model Sandwiched between Dummy Models

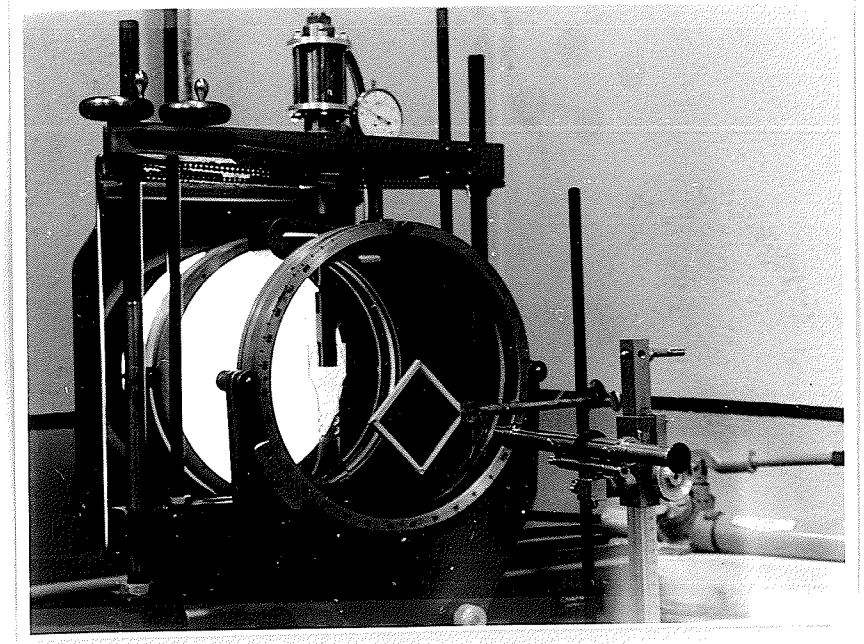

Figure 4.7 Diffused Light Type Circular Polariscope Unit,12 inch size

arangement operated by a hydraulic jack, as well as a chain drive bridging the vertical threaded rods. The load is transferred to the model by the use of chain wheel drive, being sufficient as required for a sensitive photoelastic material used, and could be regulated to any desired fraction of a load with convenience.

2. Telescope

A telescope was used to obtain very close and distinct view of the isochromatic fringe order at the boundary of the discontinuity. Figure 4.7 shows the circular polariscope, straining frame and telescope setting.

3. Camera

An Asahi Pentax camera with suitable lens was used for obtaining a photographic record of the fringe patterns in the individual models.

4.6. Testing Procedure and Observations

The testing program was divided into two phases - one carried out on models containing circular holes and the other on models containing V-notches.

The tensile load was applied to each of the models under test, through single pins located in the brass bushings in the model. Several precautions were taken to assure that the loads applied to the model were purely axial. In order to eliminate bending, twisting and load eccentricity, the model was loaded through a ball-socket joint in series with a clevis at each end of the specimen.

The elements of the circular polariscope were set (steps explained in Appendix - A) and the model was strained in the loading frame, under vertical axial tension. A green filter (Kodak Wratten #77) was used to convert the white light into a monochromatic light source (5461-A) so necessary for the formation of isochromatic fringes.

The measurement of the accurate fractional fringe order for a particular load application, at the point of stress concentration on the boundary of hole or root of notch was the most important data to be collected, as this is related by the stress-optic law in two dimensions to the stress at the boundary. Since the photoelastic compensation method was somewhat difficult to be applied at the localized point of stress concentration, it was found necessary to make precision measurement of fringe orders using the telescope. The value of load corresponding to every new increasing fringe order at the point of stress concentration was noted. However, it was always found that one side of the specimen was stressed slightly higher than the other due to small eccentricities of loading and specimen asymmetry etc. Thus there was a deviation from a desired uniform tension, and in order to eliminate this effect, an average value for the two opposite sides was taken.

The axis of the telescope was kept almost perpendicular to the plane of the model. When viewed through the telescope the hairline was set parallel to the edge of the model or the vertical axial loading direction and fairly tangential to the boundary of the hole or the curved root of the notch. As illustrated in Figure 4.8, points 1 and 2

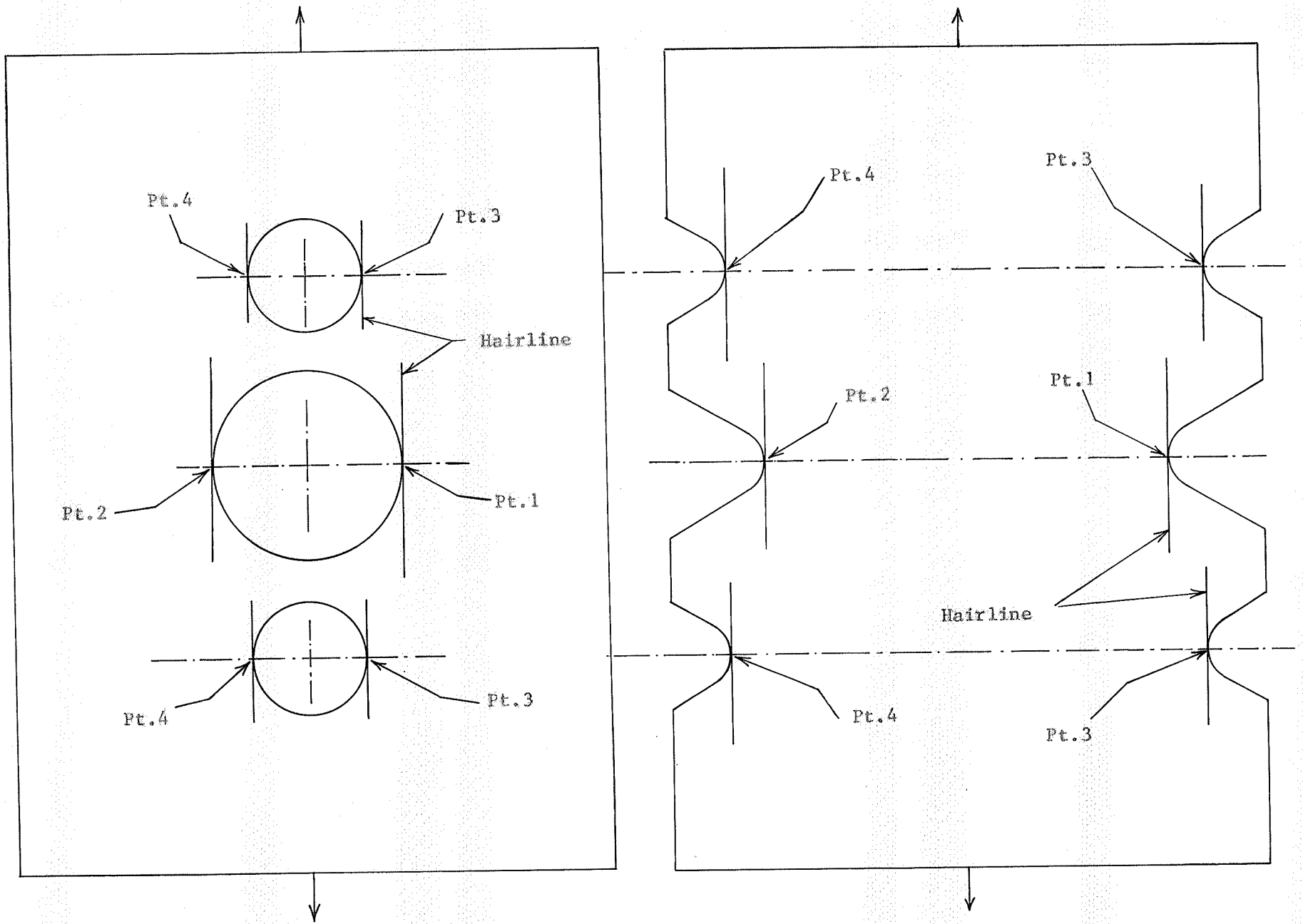

Figure 4.8 Position of Telescope Hairline Tangent to the Boundary at Point of Stress Concentration.

are the points of stress concentration on the stress raiser and points 3 and 4 are the points of stress concentration on each stress reducer. The model was stressed and for every fringe appearing at the point of stress concentration the load was noted on the dial gage provided on the loading frame of the polariscope, both when the fringe width entered the hairline and when left it to allow the new fringe to take its place. The average of the two values of the load gave the load value for the accurate mid position of the fringe at the point of stress concentration on the boundary. Proceeding this way, load readings were recorded for corresponding fringe orders both at the points 1 and 2 for stress raiser and again averaged out to a final value to minimize the error due to non-axial loading. In a similar manner the final load values were obtained by averaging out the load readings for the corresponding fringe orders at the points 3 and 4 for either stress reducer. Final load values, after averaging, corresponding to increasing fringe orders, both at raiser and reducer for a particular model are listed in separate columns in Tables 4-3 and 4-4.

Throughout the experiment, the fringe orders were measured in the dark field and so designated by numbers 1,2,3,4 etc.

4.7 Photography

As photography plays an important role in photoelastic stress analysis, it was employed to maintain a permanent record of the isochromatic fringe patterns as well as the measurement of fringe orders

TABLE 4-3

Fringe Order and Average Load Data for Various Models in Hole-Series

Fringe Order N_h	AVERAGE LOAD lb.										
	D_h = 5/16 inch; Ratio $\frac{L_h}{Dh}$ = 1										
	Model H_{10}	Model H_{11}		Model H_{12}		Model H_{13}		Model H_{14}		Model H_{15}	
	$D_h = \frac{5}{16}$ in.	$d_h = \frac{1}{16}$ in.		$d_h = \frac{1}{8}$ in.		$d_h = \frac{3}{16}$ in.		$d_h = \frac{1}{4}$ in.		$d_h = \frac{5}{16}$ in.	
	Stress Raiser	Stress Raiser	Stress Reducer	Stress Raiser	Stress Reducer	Stress Raiser	Stress Reducer	Stress Raiser	Stress Reducer	Stress Raiser	Stress Reducer
1	9.50	10.00	46.00	9.30	19.60	9.90	16.50	11.80	14.50	19.30	13.80
2	19.50	20.60	90.00	20.20	44.60	22.30	36.50	26.90	31.80	35.80	
3	32.70	33.60	134.00	32.60	70.60	35.80	57.60	41.20	50.50	52.20	42.70
4	44.40	44.20	180.00	43.90	97.20	48.80	78.80	55.10	67.50	67.10	58.20
5	56.90	56.60	226.00	56.40	123.20	61.20	96.00	69.80	84.70	83.90	72.90
6	68.40	67.70		67.60	150.00	74.40	118.80	83.00	101.70	99.70	86.90
7	79.00	78.40		80.00		87.60		97.20	119.10	113.00	100.40
8	94.80	92.40		89.60		100.80		112.00	135.20	128.00	114.80
	$D_h = \frac{5}{16}$ inch; $\frac{L_h}{dh}$ = 1.5										
	Model H_{21}			Model H_{22}		Model H_{23}		Model H_{24}		Model H_{25}	
1	9.90	23.00		9.50	14.50	10.00	16.50	11.60	12.80	15.20	13.00
2	20.40	56.20		21.00	36.00	25.10	33.80	24.50	28.30	31.80	27.60
3	32.60	89.80		33.80	58.60	34.70	51.30	39.80	43.40	47.60	41.70
4	44.80	124.00		45.30	80.30	46.90	70.00	53.80	59.20	63.20	54.60
5	55.00	159.80		57.80	100.40	60.20	87.80	69.00	73.80	79.10	66.40
6	69.00	196.40		68.90		72.50	100.80	82.60	88.50	96.60	80.70
7	81.20			82.80		84.00		95.20	102.80	112.00	94.00
8	93.60			94.00		97.40		110.00	118.40	127.00	110.40

TABLE 4-3 CONT'D

$D_h = \frac{5}{16}$ inch; $\frac{L_h}{d_h} = 2$

	Model H_{31}		Model H_{32}		Model H_{33}		Model H_{34}		Model H_{35}	
1	8.10	24.60	9.40	21.60	10.60	15.30	11.80	12.40	14.80	12.80
2	20.90	56.20	22.40	46.50	23.70	33.20	26.00	27.30	30.10	26.20
3	34.60	88.40	32.20	74.80	36.70	50.40	38.50	39.60	46.30	39.90
4	46.40	117.00	49.50	101.20	49.70	67.50	55.00	55.90	63.30	52.70
5	58.80	149.60	62.40	126.20	63.80	85.70	69.10	70.80	81.70	66.50
6	72.00	181.00	75.60	151.00	76.50	101.60	83.50	84.00	99.40	78.50
7	84.30		87.60		90.40		97.20	98.20	114.40	91.00
8	98.40		101.80		104.00		113.00	113.80		104.40

TABLE 4-4

Fringe Order and Average Load Data for Various Models in Notch-Series

Fringe Order N_n	AVERAGE LOAD lb									
	$D_n = \frac{5}{32}$ inch; Ratio $\frac{L_n}{2D_n} = 1$									
	Model N_{10}	Model N_{11}		Model N_{12}		Model N_{13}		Model N_{14}		Model N_{15}	
	$D_n = \frac{5}{32}$ in.	$d_n = \frac{1}{32}$ in.		$d_n = \frac{1}{16}$ in.		$d_n = \frac{3}{32}$ in.		$d_n = \frac{1}{8}$ in		$d_n = \frac{5}{32}$ in.	
	Stress Raiser	Stress Raiser	Stress Reducer	Stress Raiser	Stress Reducer	Stress Raiser	Stress Reducer	Stress Raiser	Stress Reducer	Stress Raiser	Stress Reducer
1	7.40	6.50	21.50	9.30	17.20	9.50	10.80	10.50	8.80	10.30	6.30
2	18.20	17.90	48.50	21.10	36.80	22.60	28.50	24.10	20.30	25.40	17.70
3	28.60	28.10	79.30	31.60	56.50	35.30	45.00	38.20	33.40	39.70	29.20
4	39.20	38.20	114.80	43.00	75.00	48.60	61.80	51.10	46.40	52.40	40.00
5	47.60	51.40	146.00	52.80	96.80	60.20	77.60	67.40	58.20	69.20	52.20
6	58.00	64.00	178.40	63.00	116.00	73.80	95.60	81.00	71.60	82.60	63.60
		$D_n = \frac{5}{32}$ inch; Ratio $\frac{L_n}{2D_n} = 1.5$									
		Model N_{21}		Model N_{22}		Model N_{23}		Model N_{24}		Model N_{25}	
1		6.00	16.30	7.30	14.70	6.70	9.80	9.10	8.40	9.50	6.00
2		15.10	37.30	17.40	32.80	18.20	23.80	20.40	21.10	22.80	16.60
3		25.40	62.40	26.70	50.20	31.00	39.60	31.70	33.30	35.50	26.80
4		35.60	84.00	38.80	67.20	44.00	53.60	43.00	45.60	49.60	38.60
5		44.40	104.80	49.20	85.40	56.00	67.20	54.00	57.60	61.80	49.20
6		56.00	124.00	57.80	107.00	70.40	85.40	66.40	69.60	77.00	61.00

TABLE 4-4 CONT'D

$D_n = \frac{5}{32}$ inch ; Ratio $\frac{L_n}{2D_n} = 2$

	Model N_{31}		Model N_{32}		Model N_{33}		Model N_{34}		Model N_{35}	
1	7.10	12.00	7.60	14.00	6.60	8.40	6.40	7.30	5.20	5.10
2	19.70	30.60	18.80	32.10	17.70	20.90	17.20	18.60	16.10	13.00
3	30.70	48.80	29.50	49.00	28.20	34.90	28.20	29.60	25.40	25.60
4	42.70	68.00	40.80	67.30	38.60	47.60	40.00	40.60	35.80	36.00
5	54.20	87.20	52.00	84.40	50.80	60.80	52.00	51.80	46.20	45.00
6	64.60	107.60	61.80	103.00	63.20	74.20	64.40	63.60	57.00	54.00

at the boundary of the hole or the root of the notch by the method of extrapolation.

Since only a portion of the shank of the tension member surrounding the discontinuities was of interest, a telescopic lens in conjunction with the necessary close-up lens was used to obtain the requisite close ups. Film, filters and paper were selected on the basis of bringing out the high contrast between dark and light areas by suppressing intermediate tones. Film exposure was directly calibrated by taking a series of shots at a fixed aperture with polarized light in correspondence to a pre-determined range of exposure times. On developing the film, the best contrasted negative was chosen by visual inspection to give the calibrated correct exposure time. That exposure was used for all photographs of isochromatics taken against the polarized light. Photographic data are listed in Table 4-6.

An illustration of the typical fringe patterns observed, for instance, in models H_{23} and N_{23} can be seen in the photographic views presented in Figures 4.9 to 4.16. The fringe photographs were enlarged to a size almost four times the original size of model, all to the same scale.

TABLE 4 - 6

Photographic Data

Camera	:	35 mm Reflex Asahi Pentax. (Asahi Optical Co., Ltd., Tokyo)
Lens	:	Takumar $f/_{3.5}$ 135 mm Telescopic Lens. In combination with close up lens of +3 diopters
Filter	:	Kodak Wratten #77 (Green) for isochromatics.
Film	:	Kodak High Contrast Copy Film.
Exposure Index:		ASA 0.6
Exposure	:	Isochromatics - $f_{/3.5}$ at 7-8 seconds . Read on Stop Watch.
Printing Paper:		Ilford Multigrade, Single Weight, with #4 Ilford green filter. Paper calibrated by using Kodak Projection Print Scale for correct exposure giving a best contrast between black and white at $f_{/3.5}$.
Film Developer:		Kodak D-11.
Film & Paper Fixer	:	Kodak fixer with hardener.
Paper Developer:		Kodak Dektol Developer.

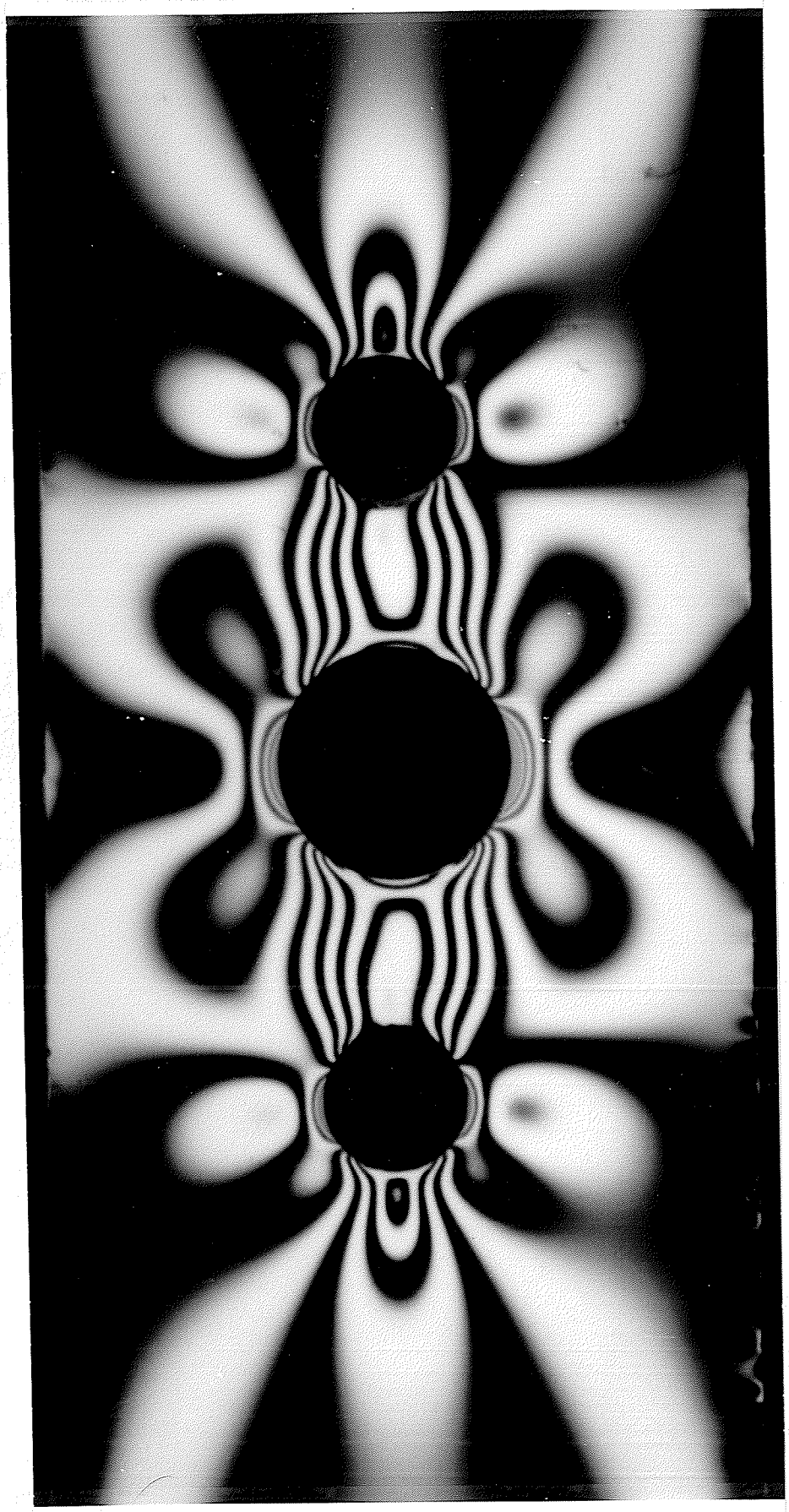

Figure 4.9 Dark Field Isochromatics in Model H_{23}
Maximum Load, P_M = 120 lb.

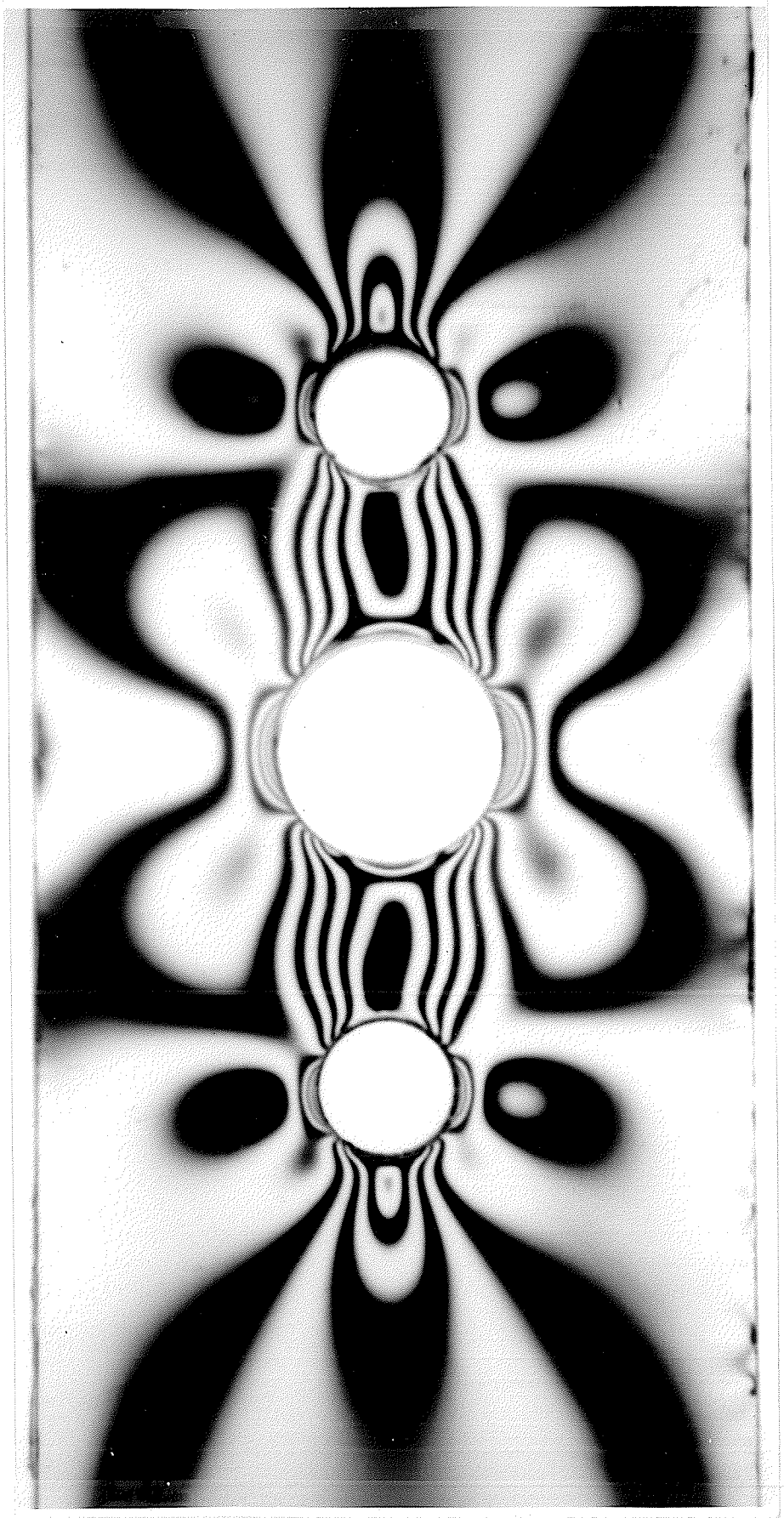

Figure 4.10 Light Field Isochromatics in Model H_{23}

Maximum Load, P_M = 120 lb.

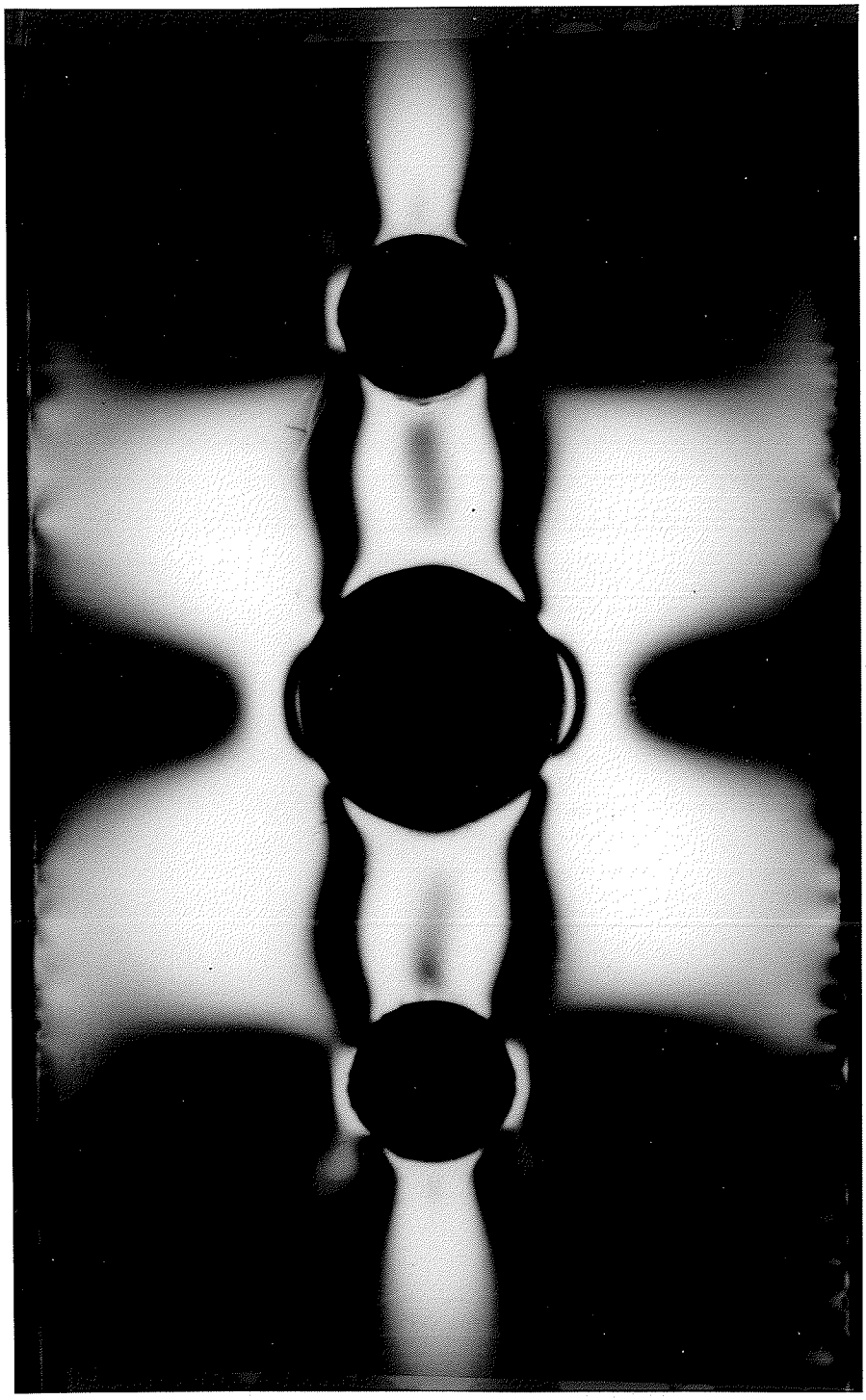

Figure 4.11 Dark Field Isochromatics in Model H_{23}
Arbitrary Zero Load, P_o = 32 lb.

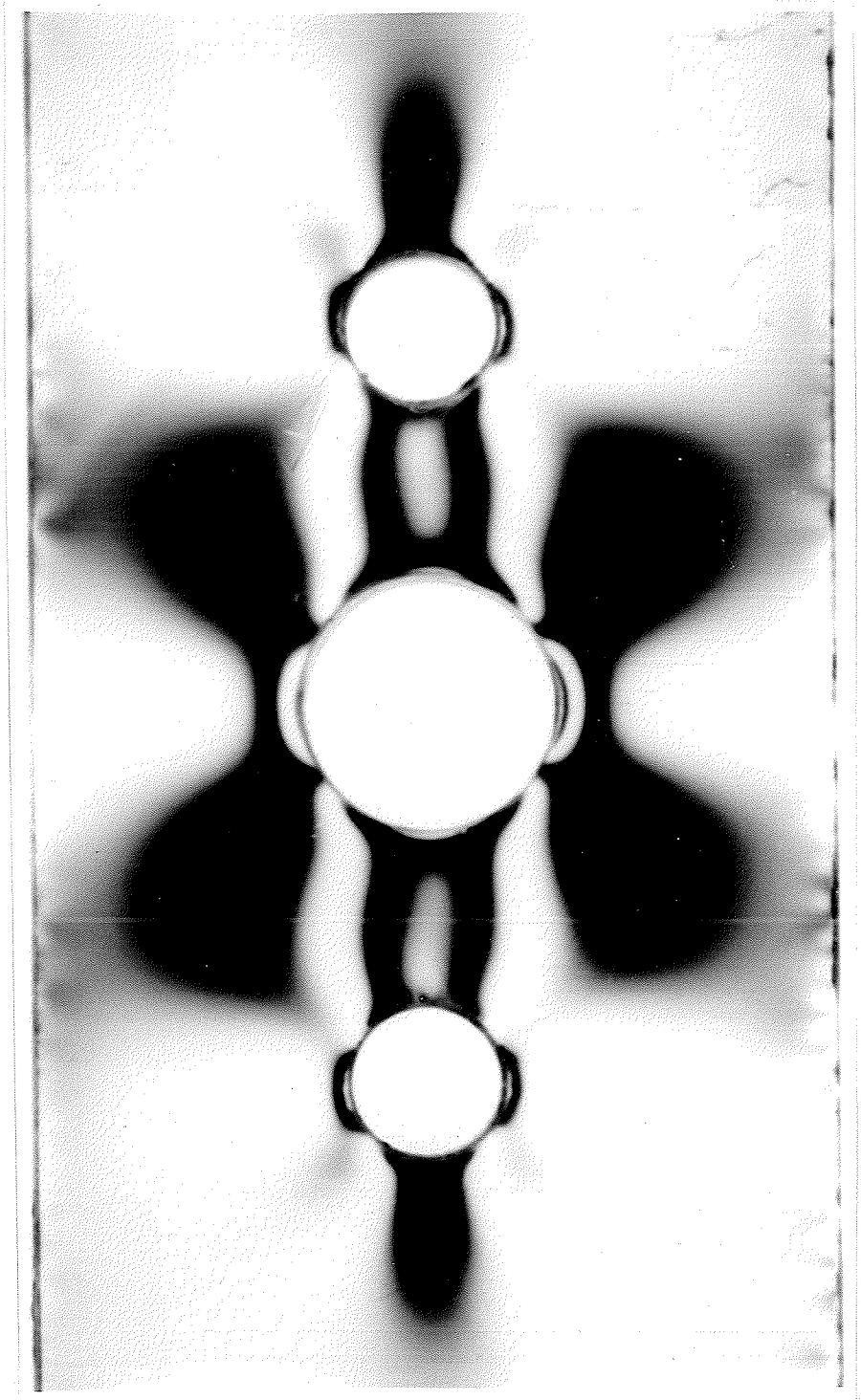

Figure 4.12 Light Field Isochromatics in Model H_{23}
Arbitrary Zero Load, P_o = 32 lb.

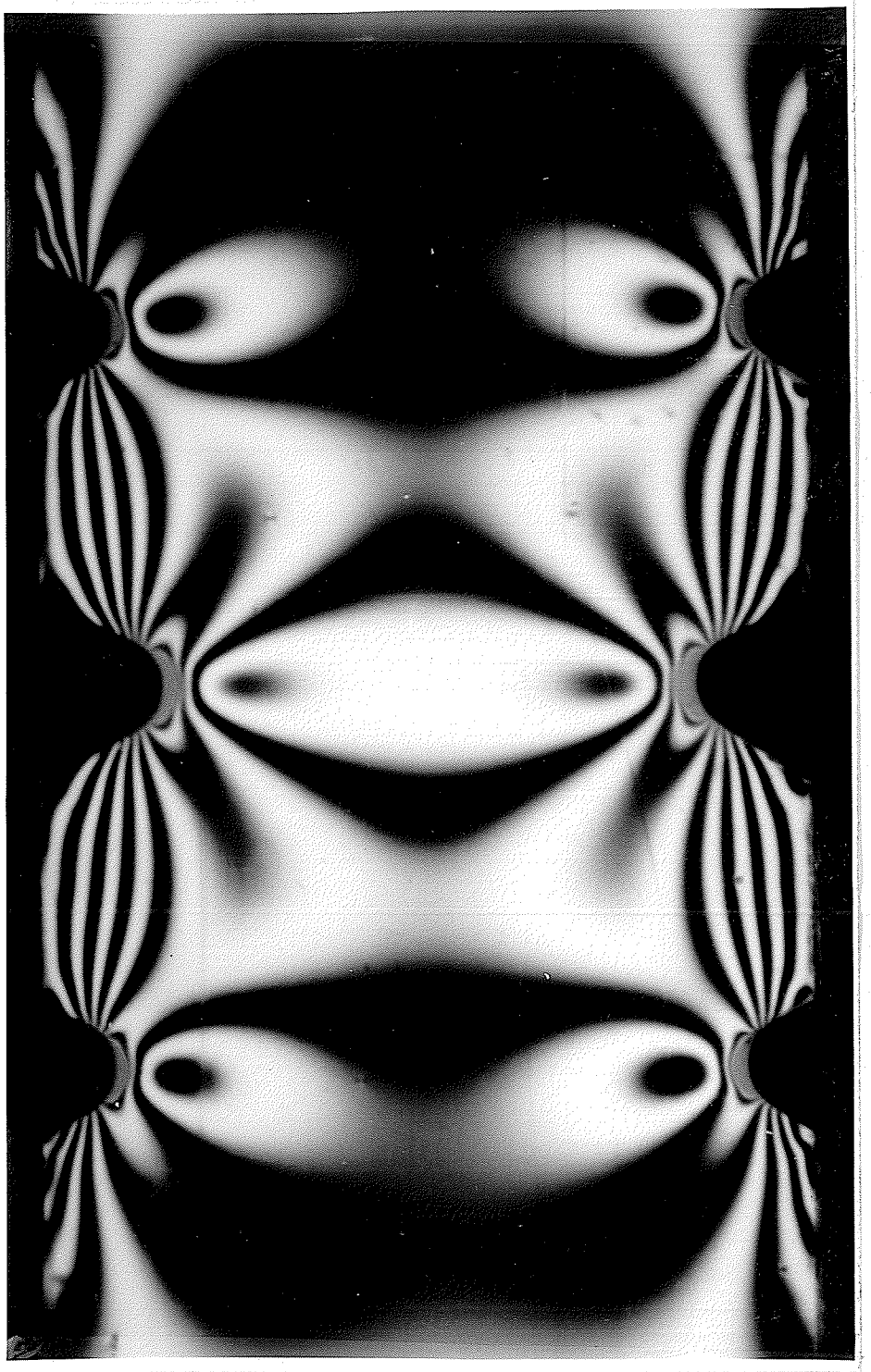

Figure 4.13 Dark Field Isochromatics in Model N_{23}
Maximum Load, P_M = 120 lb.

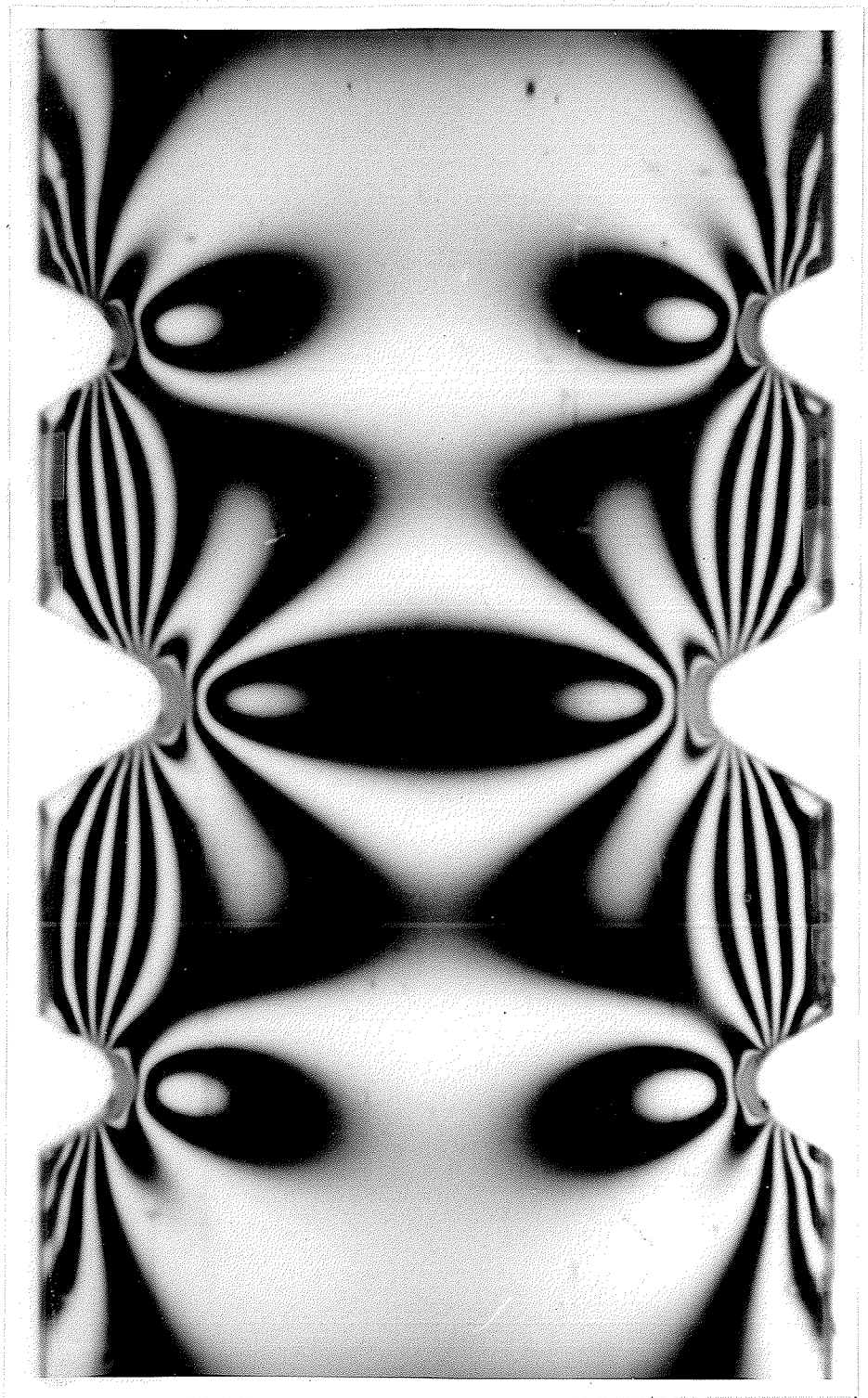

Figure 4.14 Light Field Isochromatics in Model N_{23}
Maximum Load, P_M = 120 lb.

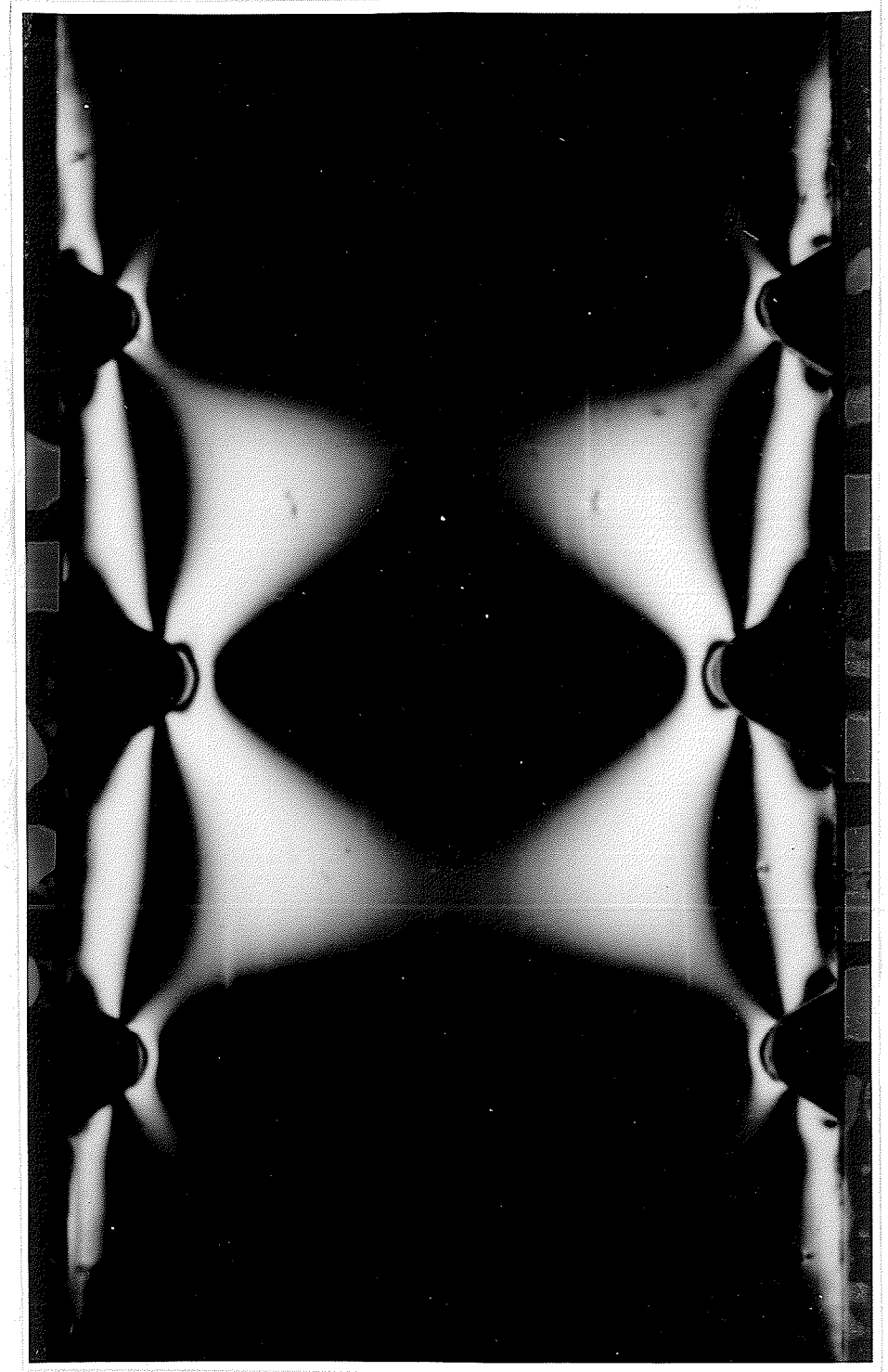

Figure 4.15 Dark Field Isochromatics in Model N_{23}
Arbitrary Zero Load, P_o = 32 lb.

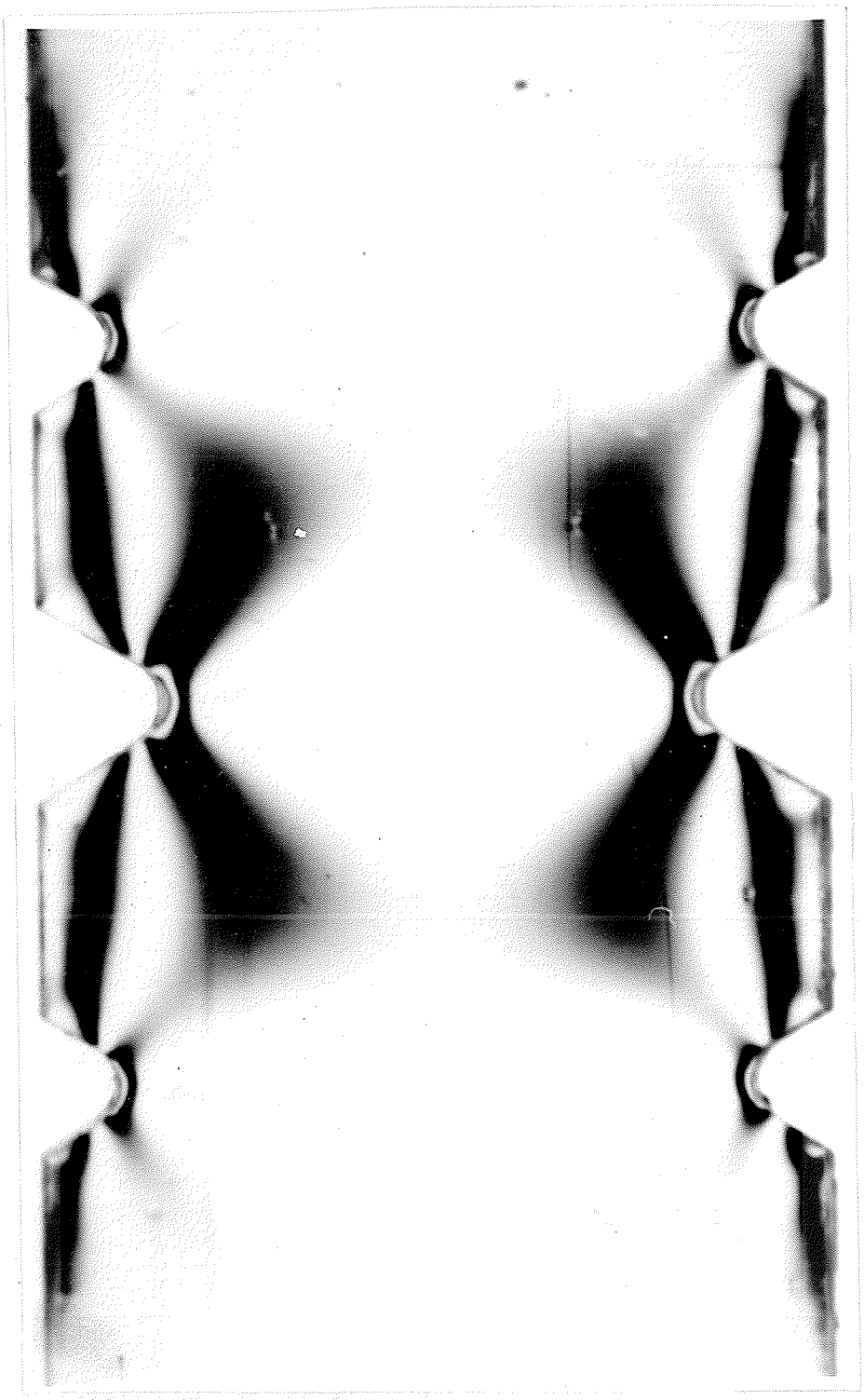

Figure 4.16 Light Field Isochromatics in Model N_{23}
Arbitrary Zero Load, P_o = 32 lb.

CHAPTER 5

ANALYSIS OF TEST RESULTS AND DISCUSSION

5.1 Introduction

The present chapter shall illustrate the interpretation of experimental test data as obtained in chapter 4, the results obtained and their analysis.

5.2 Interpretation of Test Data

1. Precise Measurement

The data in Tables 4-3 and 4-4 has been used to plot the applied load 'P'versus the fringe order 'N' for each model. The variation of load with fringe order was found to be approximately linear, separately at the stress raiser and stress reducer in the same model. From this linear plot of P versus N, the unit load fringe order was determined, after taking the average of four values from each straight line plot. The values of the unit fringe order thus obtained are shown in columns (2) and (3) for models in the Hole-series, and columns (5) and (6) for models in the notch-series with reference to Table 5-1. Employing the fringe value method as discussed in chapter 3, the values of maximum stress, σ_{max}, calculated under an arbitrary load of 100 lb; and those of theoretical stress concentration factor, K_t, are presented in Tables 5-2 and 5-3 (sample calculations are given in Appendix C). The maximum stress at the discontinuity (raiser or reducer) as a per-

TABLE 5-1

Unit Load Fringe Orders for Various Models

Unit Load Fringe Order $N_{/P}$ Measured From The Graph					
(1)	(2)	(3)	(4)	(5)	(6)
Model	Stress Raiser	Stress Reducer	Model	Stress Raiser	Stress Reducer
H_{10}	$^1/_{12.30}$		N_{10}	$^1/_{10.00}$	
H_{11}	$^1/_{11.70}$	$^1/_{44.00}$	N_{11}	$^1/_{11.20}$	$^1/_{31.20}$
H_{12}	$^1/_{11.75}$	$^1/_{26.00}$	N_{12}	$^1/_{11.30}$	$^1/_{19.366}$
H_{13}	$^1/_{12.75}$	$^1/_{21.10}$	N_{13}	$^1/_{12.866}$	$^1/_{16.80}$
H_{14}	$^1/_{14.40}$	$^1/_{17.20}$	N_{14}	$^1/_{14.00}$	$^1/_{12.334}$
H_{15}	$^1/_{15.80}$	$^1/_{14.50}$	N_{15}	$^1/_{14.534}$	$^1/_{11.40}$
H_{21}	$^1/_{12.00}$	$^1/_{34.00}$	N_{21}	$^1/_{9.80}$	$^1/_{22.2}$
H_{22}	$^1/_{12.05}$	$^1/_{21.10}$	N_{22}	$^1/_{10.20}$	$^1/_{17.638}$
H_{23}	$^1/_{12.40}$	$^1/_{17.80}$	N_{23}	$^1/_{12.466}$	$^1/_{14.534}$
H_{24}	$^1/_{14.05}$	$^1/_{15.35}$	N_{24}	$^1/_{11.40}$	$^1/_{12.30}$
H_{25}	$^1/_{15.90}$	$^1/_{13.80}$	N_{25}	$^1/_{13.35}$	$^1/_{10.60}$
H_{31}	$^1/_{12.70}$	$^1/_{31.00}$	N_{31}	$^1/_{11.80}$	$^1/_{18.634}$
H_{32}	$^1/_{13.10}$	$^1/_{26.00}$	N_{32}	$^1/_{10.60}$	$^1/_{17.375}$
H_{33}	$^1/_{13.20}$	$^1/_{17.40}$	N_{33}	$^1/_{11.066}$	$^1/_{12.866}$
H_{34}	$^1/_{14.275}$	$^1/_{14.15}$	N_{34}	$^1/_{11.40}$	$^1/_{11.06}$
H_{35}	$^1/_{16.50}$	$^1/_{13.10}$	N_{35}	$^1/_{10.35}$	$^1/_{9.675}$

TABLE 5-2

Values of σ_{max} and K_t for Models in Hole-Series

Model	Maximum Stress psi σ_{max}		Theoretical SCF K_t	
	Stress Raiser	Stress Reducer	Stress Raiser	Stress Reducer
H_{10}	1302.00		2.237	
H_{11}	1368.00	363.63	2.350	0.853
H_{12}	1362.00	615.00	2.340	1.346
H_{13}	1255.00	762.00	2.157	1.540
H_{14}	1111.00	930.00	1.908	1.743
H_{15}	1012.00	1103.00	1.742	1.898
H_{21}	1332.50	471.00	2.293	1.102
H_{22}	1327.50	758.50	2.283	1.660
H_{23}	1290.00	898.50	2.220	1.755
H_{24}	1138.00	1042.00	1.958	1.955
H_{25}	1006.00	1159.00	1.731	1.995
H_{31}	1260.00	517.00	2.167	1.210
H_{32}	1222.00	615.50	2.100	1.346
H_{33}	1212.00	919.50	2.084	1.868
H_{34}	1121.50	1130.00	1.926	2.120
H_{35}	970.00	1222.00	1.667	2.100

TABLE 5-3

Values of σ_{max} and K_t for Models in Notch-Series

Model	Maximum Stress σ_{max} psi		Theoretical SCF K_t	
	Stress Raiser	Stress Reducer	Stress Raiser	Stress Reducer
N_{10}	1600.00		2.750	
N_{11}	1428.00	513.00	2.477	1.208
N_{12}	1416.00	827.00	2.434	1.808
N_{13}	1245.00	953.00	2.138	1.934
N_{14}	1143.00	1296.00	1.964	2.432
N_{15}	1100.00	1403.00	1.893	2.413
N_{21}	1634.00	726.50	2.806	1.690
N_{22}	1569.00	921.50	2.693	1.987
N_{23}	1285.00	1102.00	2.208	2.236
N_{24}	1430.00	1301.00	2.412	2.440
N_{25}	1198.00	1510.00	2.060	2.596
N_{31}	1357.00	859.00	2.332	2.014
N_{32}	1510.00	922.00	2.593	2.016
N_{33}	1447.00	1244.00	2.488	2.528
N34	1430.00	1447.00	2.412	2.713
N_{35}	1546.00	1654.00	2.657	2.847

centage of the maximum stress at the stress raiser (for a model with stress raiser only) is given in Table 5-4.

From Tables 5-2 and 5-3, a plot of parametric curves of maximum stress versus ratio $\frac{d_h}{D_h}$ or $\frac{d_n}{D_n}$ is shown in the respective Figures 5.1 and 5.2, and those of theoretical stress concentration factor versus ratio $\frac{d_h}{D_h}$ or $\frac{d_n}{D_n}$ is shown in the respective Figures 5.3 and 5.4. Also from Table 5-4, a plot of percentage stress, $\frac{\sigma}{\sigma_m}$, versus $\frac{d_h}{D_h}$ or $\frac{d_n}{D_n}$ is shown in Figures 5.5 and 5.6. The parametric curves for respective series H_1, N_1; H_2, N_2; H_3, N_3; have been designated by A_1, A_2, A_3 in case of raiser and by B_1, B_2, B_3 in case of reducer.

2. Extrapolation

The fringe orders at the boundary of the hole or the root of the notch were also obtained from the photographs of the typical fringe patterns in the case of models in series H_2 and series N_2 only. The fringe orders in the dark field are designated in the sequence 0, 1, 2, 3, 4, etc., and in the light field by ½, 1½, 2½, 3½, 4½, etc. The singular point or the point of zero fringe order was located on the boundary of the hole or the notch in the individual photograph by close visual observation, and then extrapolated right up to the point of stress concentration on the boundary of the discontinuity. Starting with the singular point, the fringe order increased toward the tension side and decreased toward the compression side. The fringe orders thus extrapolated are shown under the columns of N_M and N_0 in Table 5-5. With reference to fringe orders $N = N_M - N_0$, under a net load $P = P_M - P_o$,

TABLE 5-4

Percentage Stress at the Discontinuity for Various Models.

	$\frac{\sigma^*}{\sigma_m}$ Percentage				
Model	Stress Raiser	Stress Reducer	Model	Stress Raiser	Stress Reducer
H_{10}	100.00		N_{10}	100.00	
H_{11}	105.20	27.90	N_{11}	89.20	32.05
H_{12}	104.80	47.30	N_{12}	88.40	51.70
H_{13}	96.50	58.50	N_{13}	77.85	59.60
H_{14}	85.40	71.50	N_{14}	71.50	81.00
H_{15}	77.75	84.85	N_{15}	68.75	87.75
H_{21}	102.40	36.80	N_{21}	102.10	45.35
H_{22}	102.00	58.30	N_{22}	98.00	57.60
H_{23}	99.25	69.00	N_{23}	80.35	68.80
H_{24}	87.60	80.20	N_{24}	89.40	81.35
H_{25}	77.35	89.10	N_{25}	74.90	94.40
H_{31}	96.90	39.76	N_{31}	84.80	53.70
H_{32}	94.00	47.30	N_{32}	94.40	57.65
H_{33}	93.20	70.70	N_{33}	90.40	77.80
H_{34}	86.20	86.85	N_{34}	89.40	90.40
H_{35}	74.65	93.90	N_{35}	96.60	103.40

The stresses defined below refer to corresponding series.

* σ = Maximum stress at the discontinuity (Raiser or Reducer) for all models other than H_{10} or N_{10}

σ_m = Maximum stress at the discontinuity for model H_{10} or N_{10}

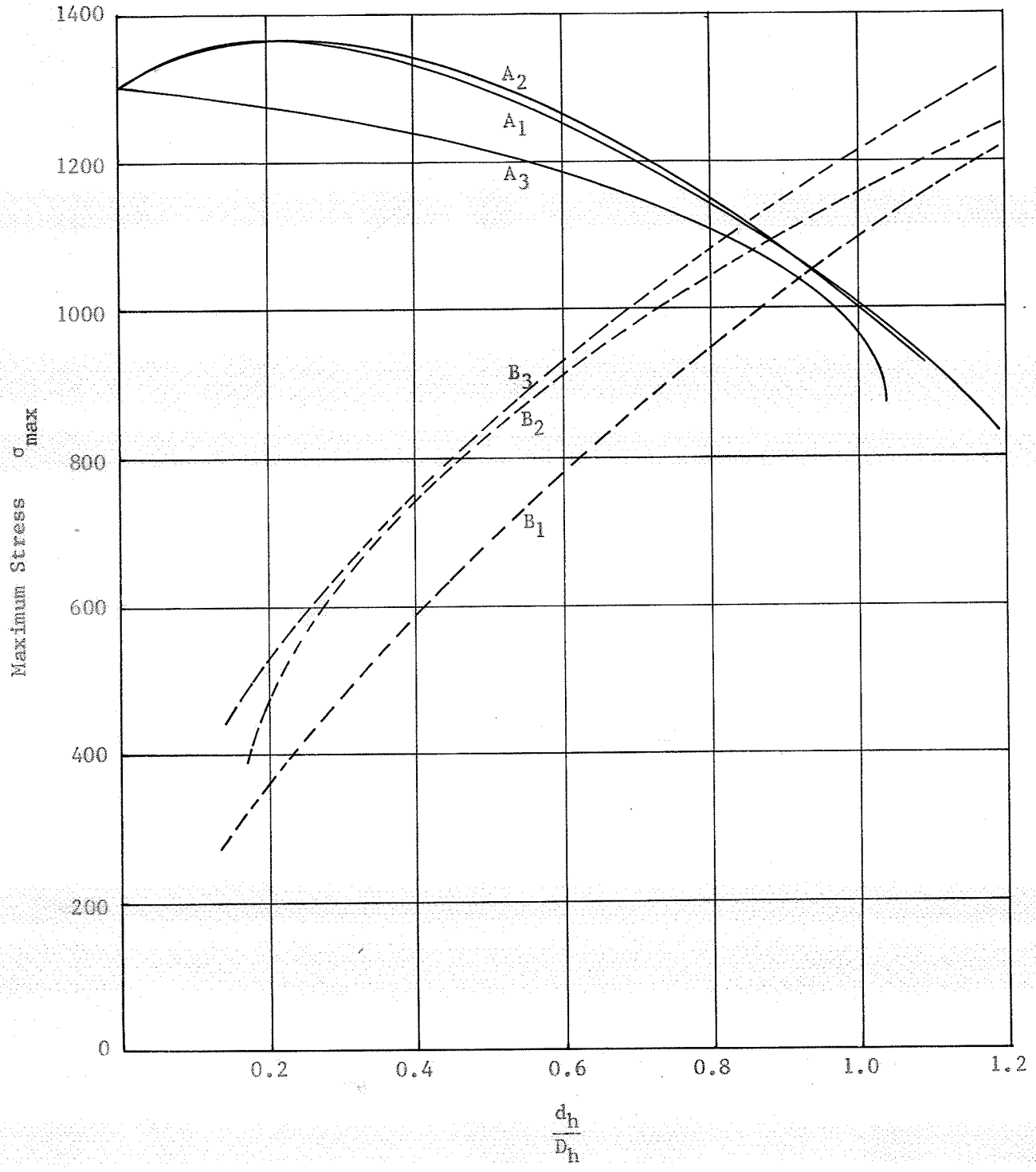

Figure 5.1 Maximum Stress for Models in Series H_1, H_2, H_3 drawn on Comparative Basis.

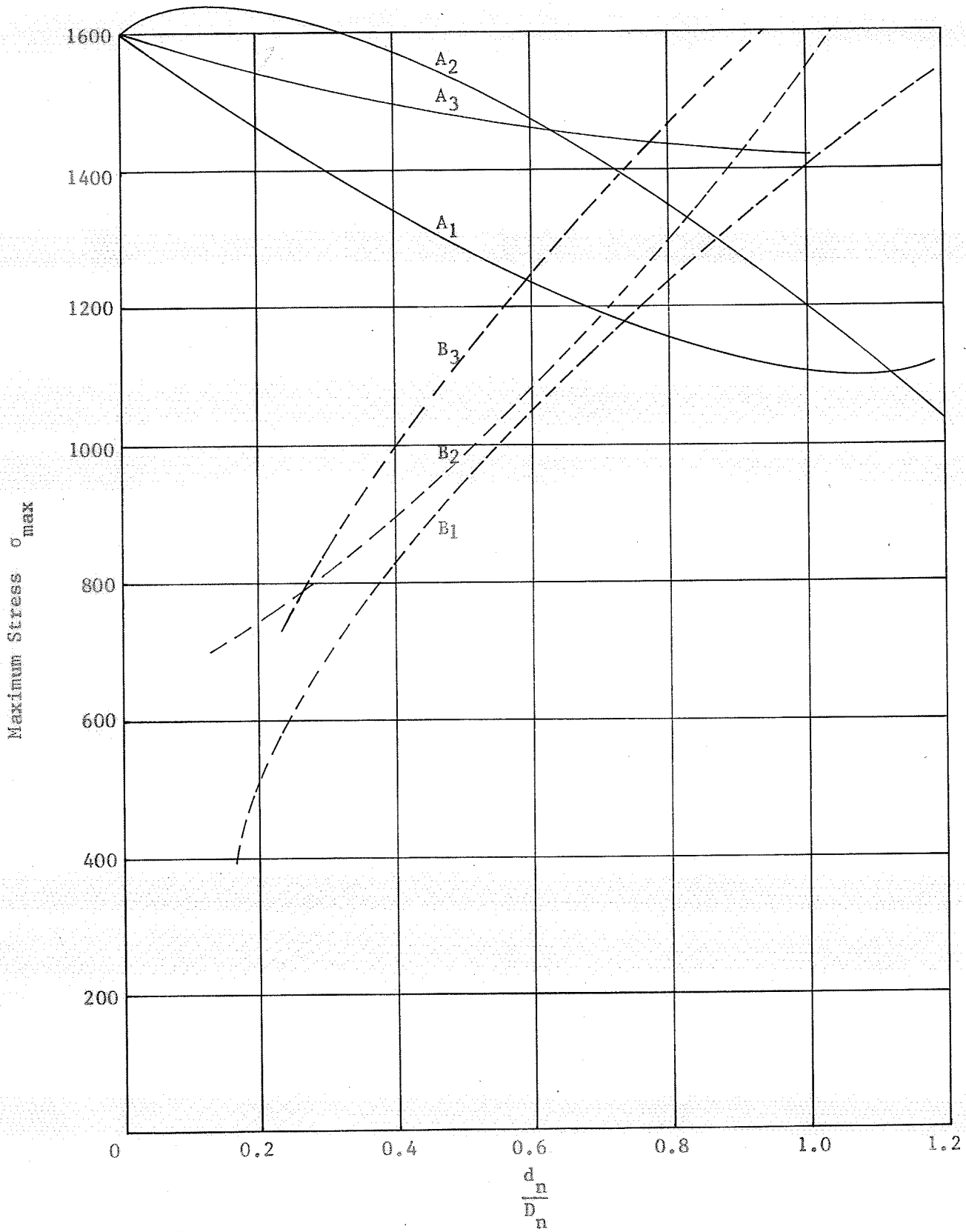

Figure 5.2 Maximum Stress for Models in Series N_1, N_2, N_3 drawn on Comparative Basis.

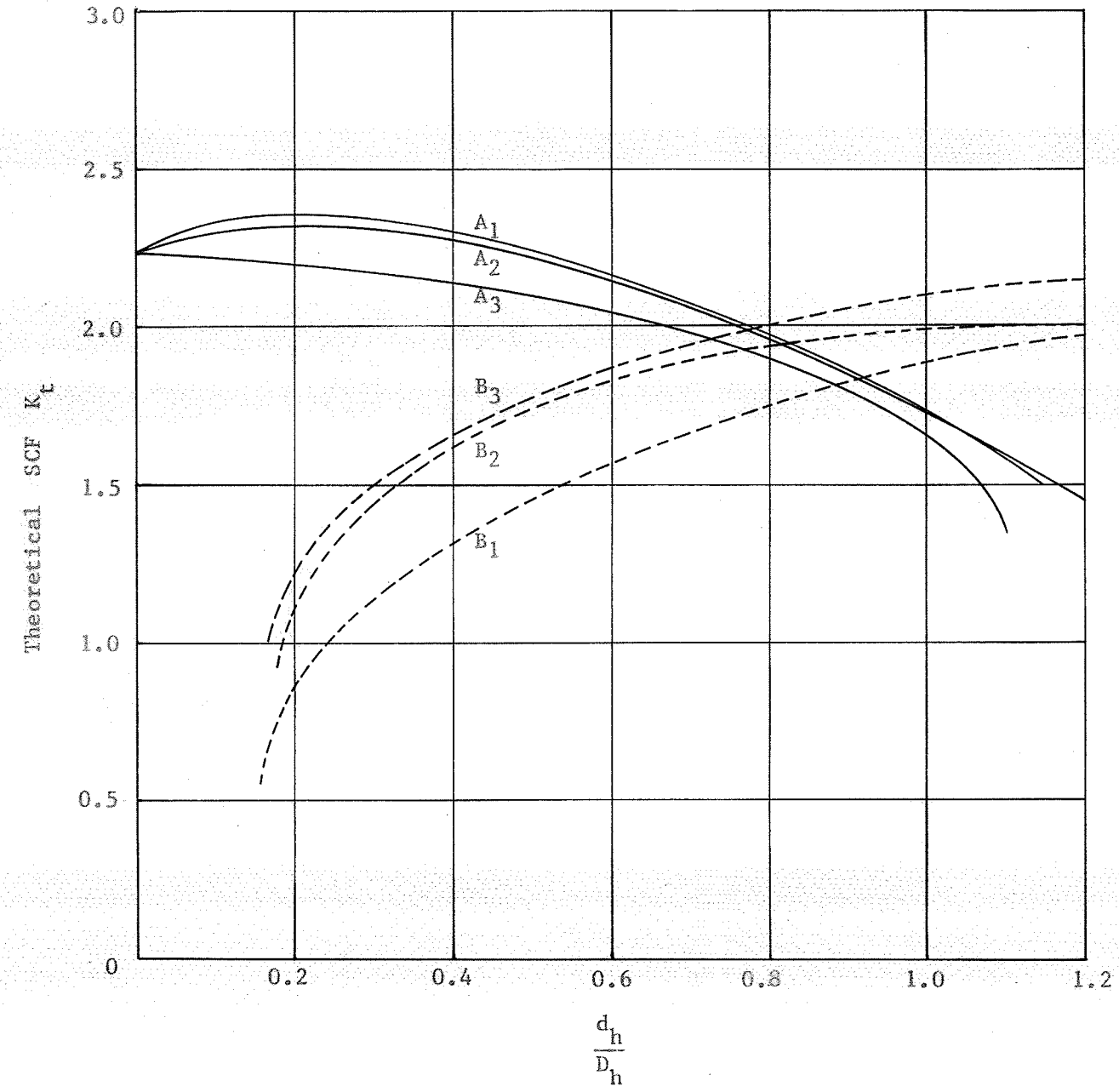

Figure 5.3 Theoretical Stress Concentration Factors for Models in Series H_1, H_2, H_3, drawn on Comparative Basis.

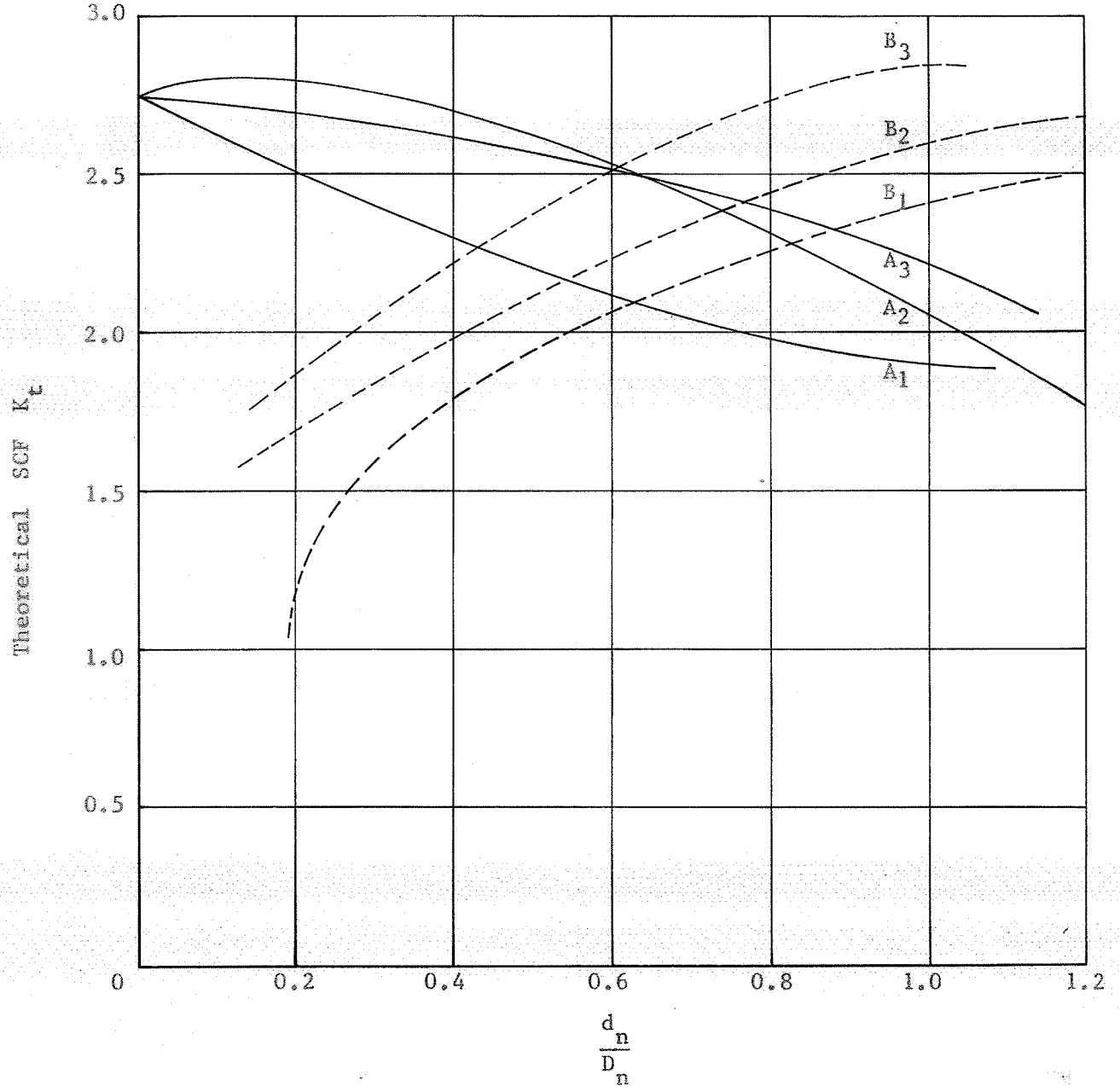

Figure 5.4 Theoretical Stress Concentration Factors for Models in Series N_1, N_2, N_3, drawn on Comparative Basis.

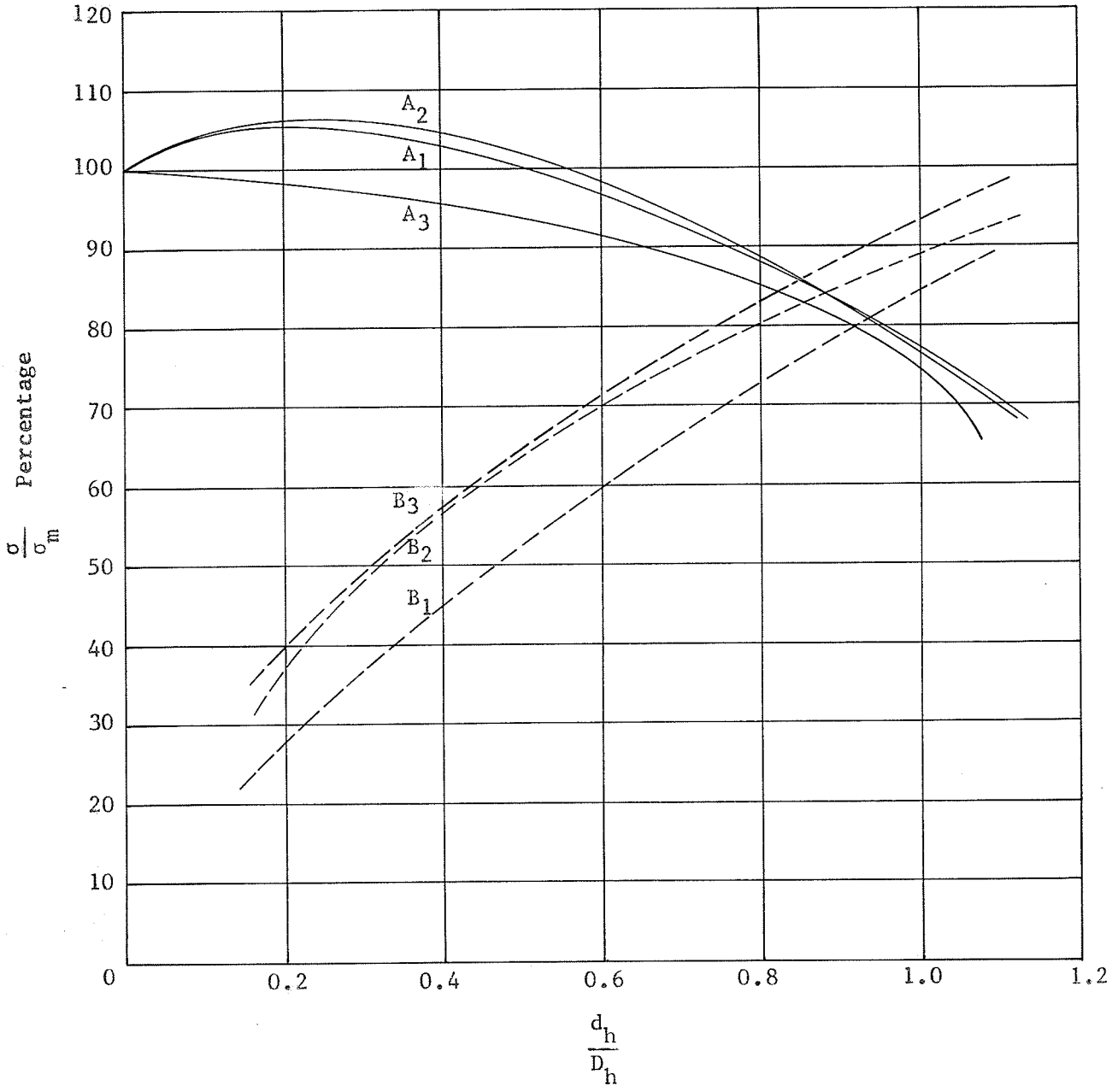

Figure 5.5 Percentage Stress at the Discontinuity for Models in Series H_1, H_2, H_3.

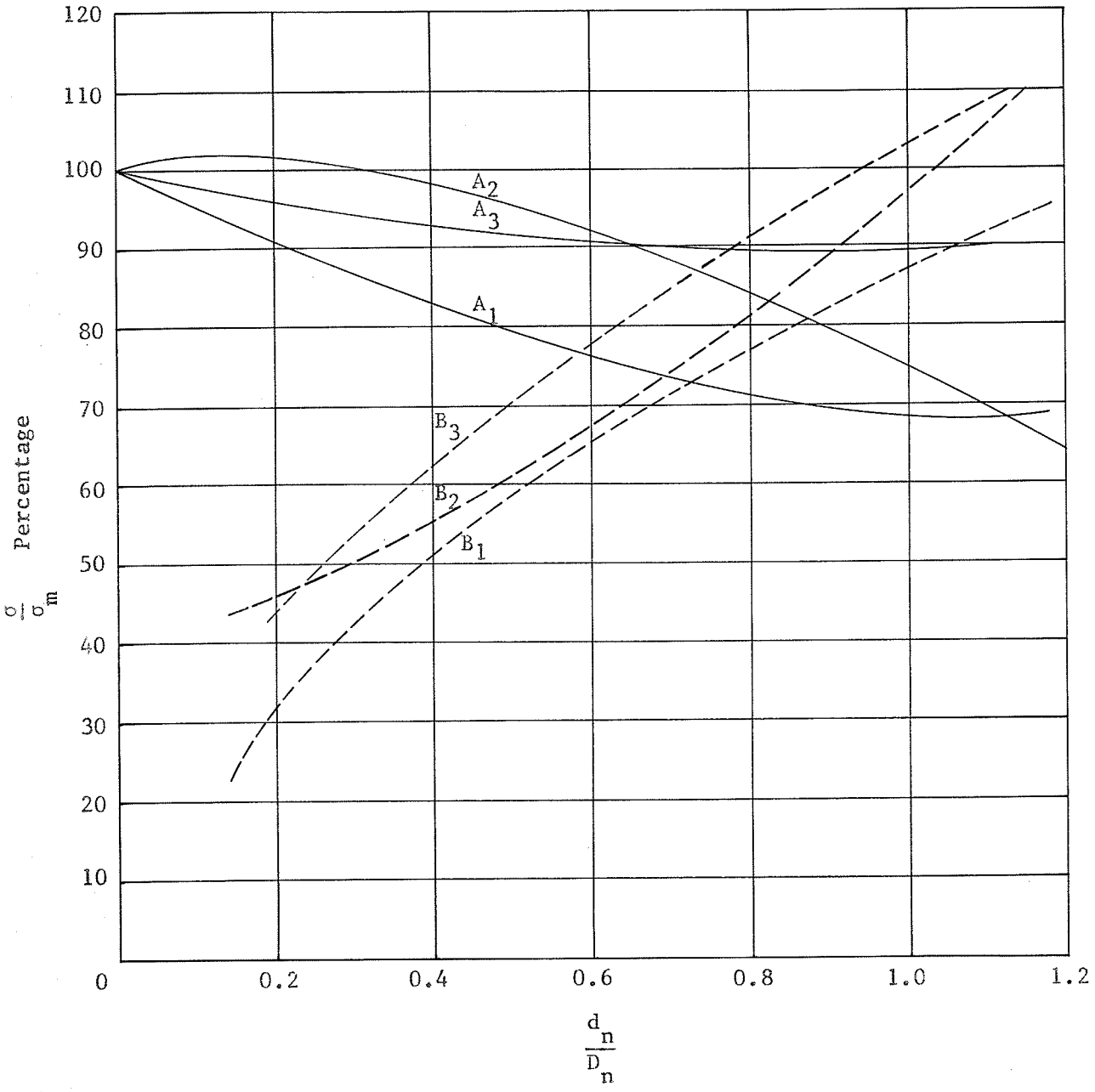

Figure 5.6 Percentage Stress at the Discontinuity for Models in Series N_1, N_2, N_3.

TABLE 5-5

Measurement of Fringe Orders by Extrapolation

Model	Fringe Order at the Point of Stress Concentration on the Boundary					
	N_M		N_o		$N = N_M - N_o$	
	Under Maximum Load, P_M= 120lb.		Under Arbitrary Load, P_o= zero 32lb.		Under Net Load $P_M - P_o$=88lb.	
	Stress Raiser	Stress Reducer	Stress Raiser	Stress Reducer	Stress Raiser	Stress Reducer
H_{10}	9.0		2.8		6.2	
H_{21}	11.0	3.0	2.7	1.5	8.3	1.5
H_{22}	10.0	5.5	2.8	2.0	7.2	3.5
H_{23}	9.5	5.7	3.0	2.0	6.5	3.7
H_{24}	8.5	7.5	2.5	2.1	6.0	5.4
H_{25}	7.5	9.0	2.0	2.6	5.5	6.4
N_{10}	12.0		3.5		8.5	
N_{21}	11.7	4.0	3.4	0.5	8.3	3.5
N_{22}	11.3	6.5	3.3	2.5	8.0	4.0
N_{23}	11.0	8.5	3.3	2.6	7.7	5.9
N_{24}	10.5	10.5	3.2	2.7	7.3	7.8
N_{25}	10.0	11.5	3.0	3.0	7.0	8.5

as listed in this table, the values of σ_{max} and K_t were calculated (sample calculations are given in Appendix C). The values of σ_{max} were also calculated for arbitrary load of 100 lb. for purposes of comparison with the corresponding values found by precise measurement method. The above mentioned values are listed in Table 5-6. The parametric curves of maximum stress and theoretical stress concentration factor (found by extrapolation) drawn separately, versus $\frac{d_h}{D_h}$ or $\frac{d_n}{D_n}$, and also on comparative basis with precise measurement are shown in Figures 5.7 to 5.10.

The parametric curves for series H_2, N_2 have been designated by a_2 in case of raiser and by b_2 in case of reducer.

5.3 Discussion of Results

The observations on experimental results show that the theoretical stress concentration factor for a single circular hole in a uniaxial tension member of finite width is 2.237 (for Model H_{10} in Table 5-2) by precise measurement. This value compares nearly with the value 2.35 obtainable from the already existing curve in Figure 3.5, the value 2.28 found with photoelastic experiments by Frocht [12] and also 2.32 found by Wahl and Beeuwkes [13]. The value 1.937 (for Model H_{10} in Table 5-6) found by extrapolation of the photographs differs somewhat from the accepted values. For this reason it has been assumed that more accurate results were obtained by precise measurement method than by extrapolation.

TABLE 5-6

Values of σ_{max} and K_t by the Method of Extrapolation

MODEL	MAXIMUM STRESS σ_{max} - psi				THEORETICAL SCF K_t	
	Under Net Load P = 881b.		Under Arbitrary Load P = 100 lb.			
	Stress Raiser	Stress Reducer	Stress Raiser	Stress Reducer	Stress Raiser	Stress Reducer
H_{10}	993.00		1128.00		1.937	
H_{21}	1330.00	241.00	1512.00	274.00	2.593	0.640
H_{22}	1153.00	561.00	1310.00	637.00	2.250	1.394
H_{23}	1041.00	592.50	1183.00	672.00	2.030	1.367
H_{24}	962.00	865.00	1092.50	983.00	1.875	1.843
H_{25}	881.00	1026.00	1002.00	1165.00	1.718	2.00
N_{10}	1362.00		1546.00		2.656	
N_{21}	1330.00	560.00	1512.00	636.00	2.593	1.490
N_{22}	1282.00	641.00	1456.00	728.00	2.500	1.593
N_{23}	1233.00	945.00	1403.00	1073.00	2.407	2.180
N_{24}	1169.00	1249.00	1328.00	1420.00	2.282	2.662
N_{25}	1121.00	1362.00	1273.00	1547.00	2.187	2.658

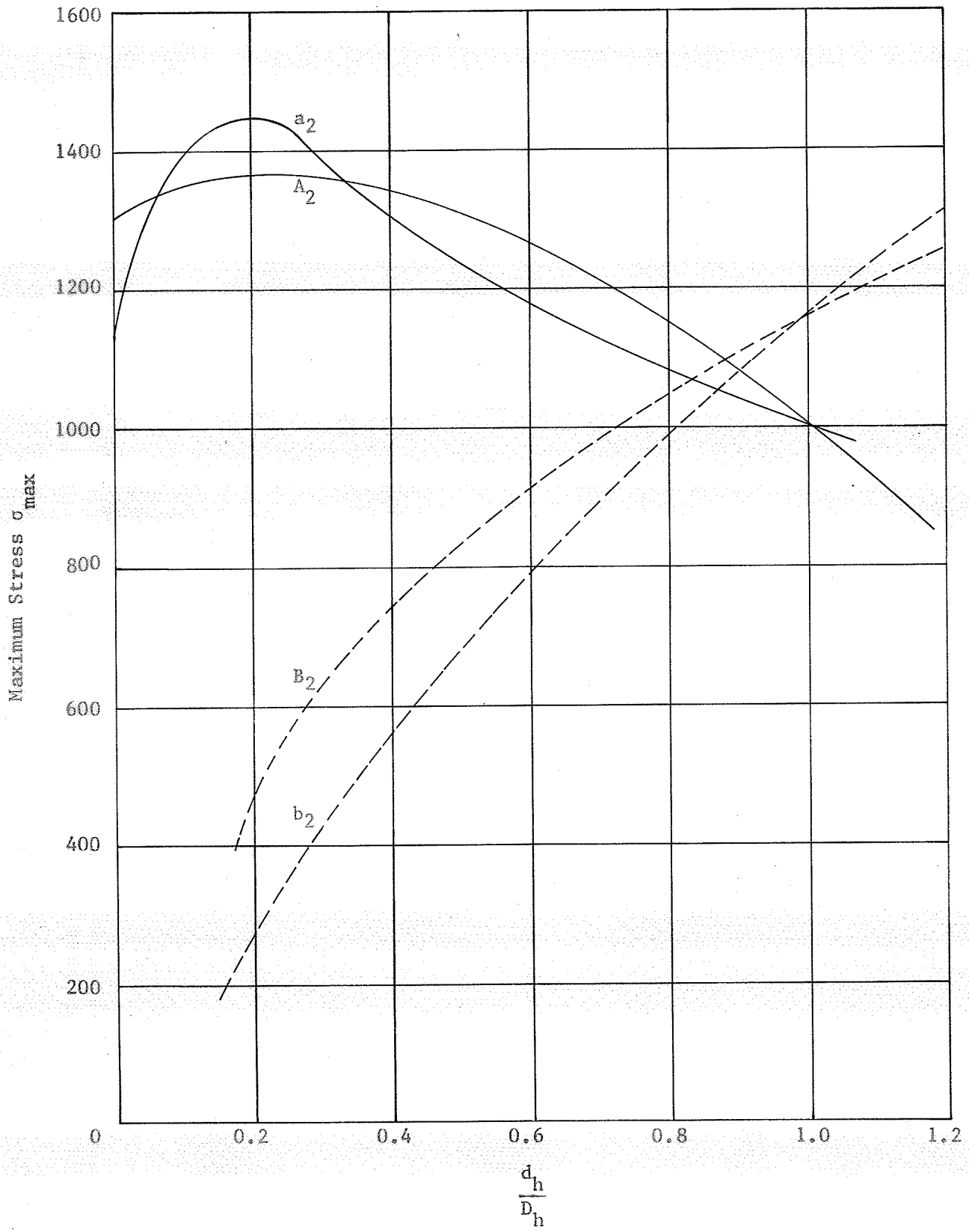

Figure 5.7 Maximum Stress for Models in Series H_2, compared by Precise Measurement (curves A_2, B_2) and Extrapolation (curves a_2, b_2).

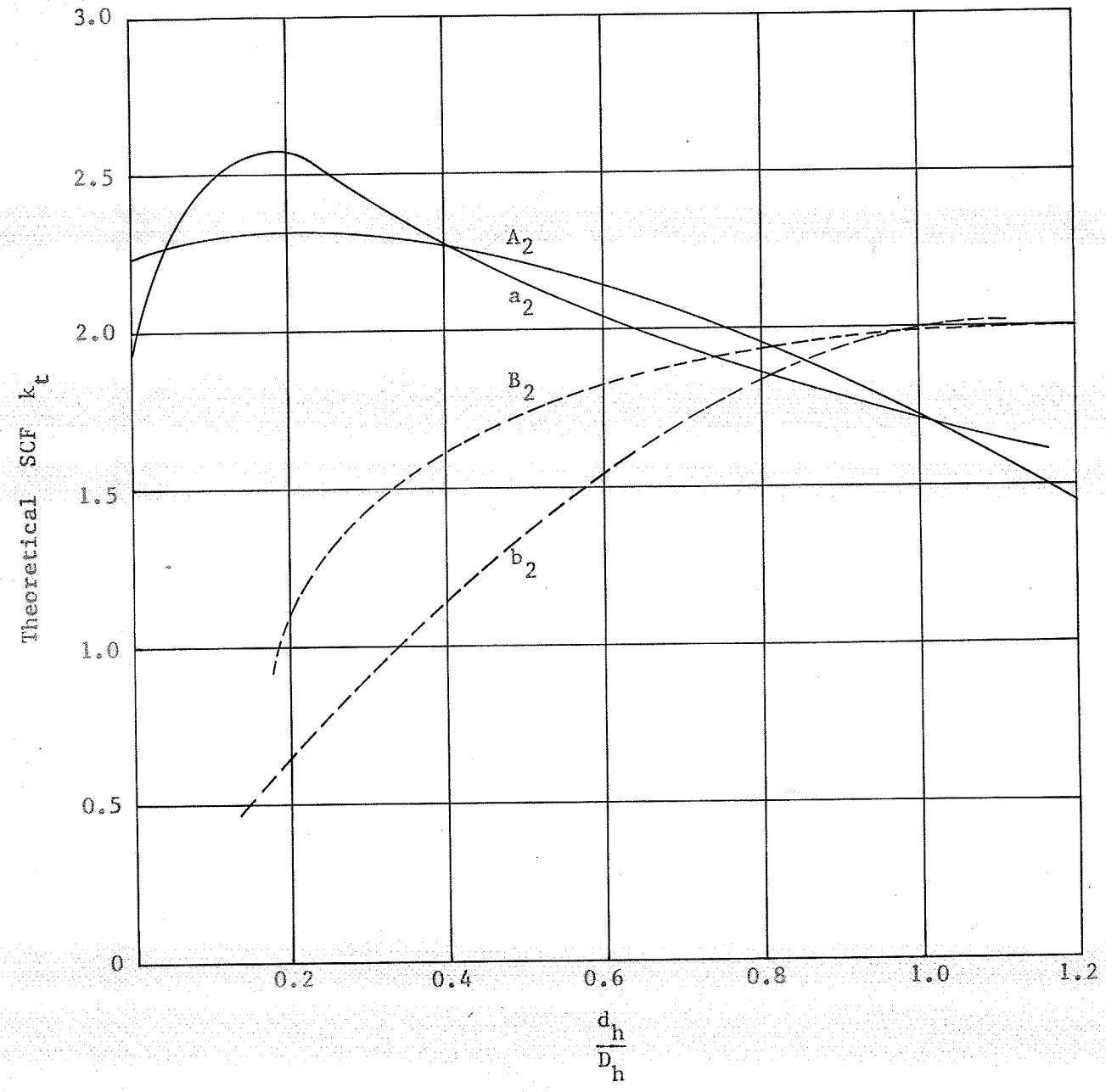

Figure 5.8 Theoretical Stress Concentration Factors for Models in Series H_2 compared by Precise Measurement (curves A_2, B_2) and Extrapolation (curves a_2, b_2).

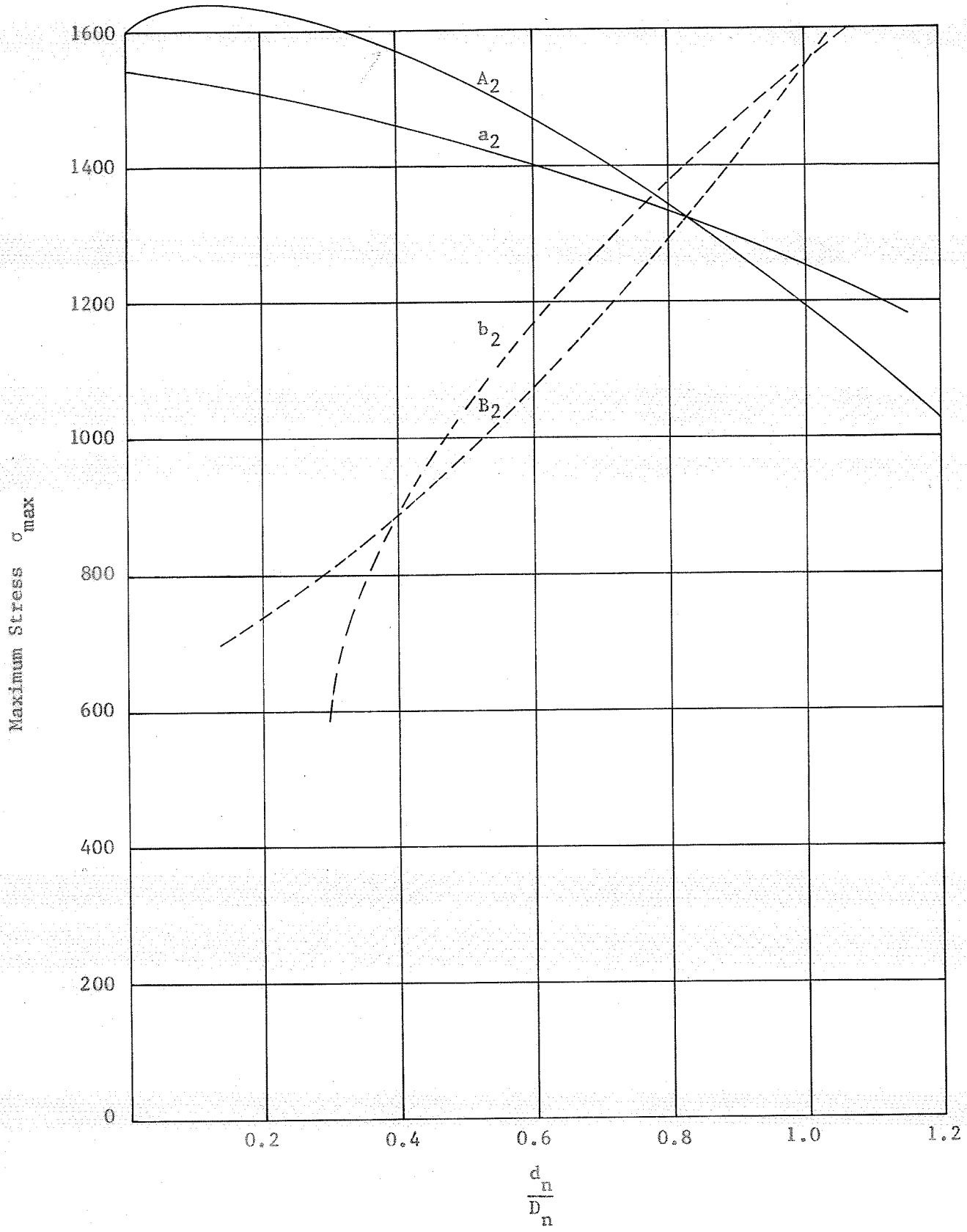

Figure 5.9 Maximum Stress for Models in Series N_2 compared by Precise Measurement (curves A_2, B_2) and Extrapolation (curves a_2,b_2).

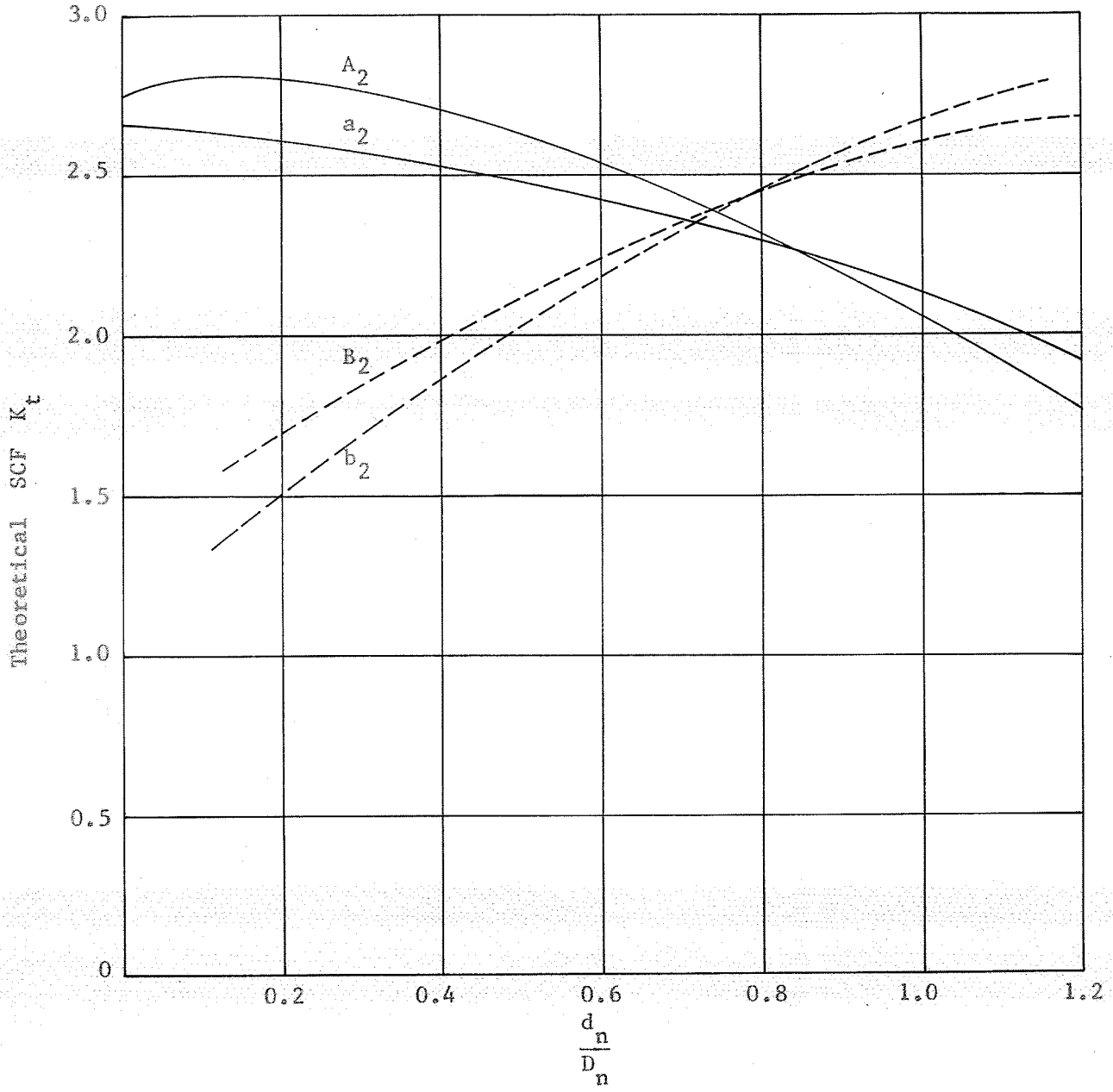

Figure 5.10 Theoretical Stress Concentration Factors for Models in Series N_2 compared by Precise Measurement (curves A_2,B_2) and Extrapolation (curves a_2,b_2).

The stress concentration factor for double symmetrical V-notches (acting as stress raiser only) in a uniaxial tension member of finite width was obtained as 2.75 (for Model N_{10} in Table 5-3). This differs somewhat from the published [64] value, 3.22. The value 2.656 (for Model N_{10} in Table 5-6) was obtained by extrapolation.

The effect of material removal in the neighbourhood of constant size stress raiser, by means of the introduction of stress reducers of increasing sizes can be seen in the following facts.

At a point of stress concentration on the boundary of stress raiser, the maximum stress and so also the theoretical stress concentration factor have a declining trend (parametric curves A_1 or A_2 or A_3 in Figures 5.1 to 5.6 or curve a_2 in Figures 5.7 to 5.10) with increasing size of stress reducer. On the other hand, the stress concentration factor in the reducer increases with reducer size. The parametric curves for stress raiser tend to bulge up in some cases during the initial stages of material removal indicating increase of stress concentration. One reason for this may be the measurement of slope of graph P Vs N, slight variation of which may change the fringe order per lb. of load thus affecting the value of stress concentration factor. Another reason may be the interdependence of stress raiser and stress reducers of different relative sizes when in co-existence.

It is seen that the curves for stress raiser and stress reducer have reverse inclinations and, therefore, happen to intersect at an optimum point where the values of either the maximum stress or that of stress concentration factor are the same. It is this optimum

point which is of most importance resulting in a belief that a specific amount of material removed leads to substantial reduction of stress concentration around the stress raiser without any danger of the stress exceeding the optimum limit around the stress reducer. The values of stress concentration at the optimum point and their percentage reduction from the corresponding original values obtained for stress raiser only (Models H_{10} and N_{10}) depicted by parametric curves of different series, are presented in Table 5.7.

The optimum values for series H_1, H_2 and H_3 shown comparatively in Figures 5.1, 5.3 and 5.5 illustrate that the maximum percentage reduction of stress concentration is in the case of series H_1 (Table 5-7). Also, the optimum values for series N_1, N_2 and N_3 shown comparatively in Figures 5.2, 5.4 and 5.6 illustrate that the maximum reduction of stress concentration is in the case of series N_1 (Table 5-7). Figures 5.7 to 5.10 compare the parametric curves obtained separately by precise measurement and extrapolation in case of two different series H_2 and N_2, from where, it has been observed that there is a greater percentage reduction obtained by precise measurement than by extrapolation (Table 5-7).

Finally, the experimental investigation suggests that the series H_1 and N_1 are separately the best conditions for optimum results of stress concentration reduction in case of holes and notches respectively indicating that the pitch between stress raiser and stress reducers plays a significant role to cause maximum interference of like discontinuities resulting in a greater reduction of stress concentration. Also, it has been observed on the comparison of best results of reduction in

TABLE 5-7

Optimum Values and Percentage Reduction of Stress Concentration from the Corresponding Original Values for Stress Raiser only.

	Series	Figure No.	OPTIMUM VALUES		PERCENTAGE REDUCTION FROM ORIGINAL VALUE		Ratio
			Maximum stress psi	Stress concentration factor	Maximum stress	Stress concentration factor	$\frac{d}{D}$
Precise Measurement	H_1	5.1	1054.00	1.84	19.05	17.75	0.940
		5.3					0.923
	H_2	5.1	1092.00	1.94	16.14	13.28	0.882
		5.3					0.820
	H_3	5.1	1100.00	1.96	15.52	12.38	0.825
		5.3					0.732
	N_1	5.2	1177.00	2.09	26.45	24.00	0.735
		5.4					0.626
	N_2	5.2	1328.00	2.38	17.00	13.45	0.827
		5.4					0.739
	N_3	5.2	1436.00	2.51	10.25	8.73	0.772
		5.4					0.600
Extrapolation	H_2	5.7	1052.00	1.85	6.74	4.49	0.868
		5.8					0.813
	N_2	5.9	1350.00	2.345	12.69	11.72	0.768
		5.10					0.723

case of series H_1 and N_1 (Table 5-7) that the percentage reduction of stress concentration is more pronounced in case of notches than in the case of holes. Possibly, this is because of the interference being more effective in case of notches than for holes.

Main source of error if any, to the correctness of fringe order at the boundary of discontinuity can be residual stresses in the photoelastic material employed and secondly the machining stresses introduced in some cases, though care was taken to eliminate them as far as possible. Since the error would be systematic it would not influence the data as the comparative studies were the main purpose of the test programme.

CHAPTER 6

APPLICATION OF EXPERIMENTAL RESULTS AND CONCLUSIONS

6.1 Applications

The results of the photoelastic tests carried out in this thesis can find useful application in the solution of practical design problems. The parametric curves illustrating the effect of material removal on stress concentration at a stress raiser can act as a good source of guidance to the improvement of fatigue strength where a small decrease in stress will result in a much higher fatigue life. Further investigations on different sizes of stress raiser, also with different amounts of pitch between stress raiser and each stress reducer can help in the evolution of new forms of parametric curves of optimum strength against specific amounts of material removal. Such curves can act as standard reference curves for application to design analysis with economical use of material.

As a particular application, the model studies of holes can equally well be applied to the cases of pin loaded holes. For instance, in case of a fastened structure, Smith [65] employed a thin auxiliary doubler to transfer load from a critically loaded fastener to a less critically loaded intermediate fastener thus making the pin loaded hole (with reduced stress concentration) to act more like the unloaded hole. In such a case, stress reducers (material removal) introduced

in the vicinity of a pin loaded hole and in the direction of load application should be able to share load and lower stress concentration at a critically loaded fastener.

6.2 Conclusions

The experimental investigation described in this thesis resulted in a concept that there is a definite reduction of stress concentration until a certain optimum stage, around a constant size of stress raiser by introducing stress reducers (material removal) of varying sizes in its neighbourhood. Only a limited number of parameters were studied separately for circular holes and V-notches. The two parameters, first being pitch of like discontinuities i.e., spacing between stress raiser and each stress reducer; and another, the depth of discontinuity i.e., diameter of stress reducer hole or depth of stress reducer notch, had their independent effects of reduction on stress concentration. Out of the cases dealt with, the smallest pitch corresponding to $\frac{L_h}{D_h} = 1$ and $\frac{L_n}{2D_n} = 1$ gave the most optimum results for maximum percentage reduction of stress concentration separately for holes and notches.

Though the results obtained by precise measurements in all series proved more favourable, those derived by extrapolation for series H_2 and N_2 were a good source of comparison with the corresponding series found by precise measurement. The only reason for variation could be the difficulty in measuring a very accurate fringe order by

extrapolation, because the fringes in some photographs were not distinctly defined near the point of stress concentration.

6.3 Suggestions for Further Study

Confirmations of stress concentration reduction by the present unique approach of material removal to obtain optimum stress concentration with the help of parametric curves opens a new course of investigation on more or less similar lines. The following variations of the basic problem may be considered for further research in reduction of stress concentration.

1. Cases of semi-circular notches, fillets under uniaxial tension.
2. Variation of angle and root radius of stress reducer V-notch with constant depth.
3. Effect of number of stress reducers in the vicinity of stress raiser.
4. Effect of reinforcement around the boundary of discontinuity in conjunction with material removal.
5. Every new geometrical shape of stress reducer different from that of stress raiser, causing reduction of stress concentration around the stress raiser seems to be a challenging proposition in itself.
6. Loading conditions different from uniaxial tension require individual attention.

BIBLIOGRAPHY

1. Wang, C. T., Applied Elasticity, McGraw-Hill Book Company, New York, 1953.

2. Timoshenko, S., Stress Concentration in the History of Strength of Materials, Proc. SESA, 12, 1, 1-12, 1954; AMR 8(1955), Rev. 2646.

3. Föpple, A., Dauerversuche Von Bauschinger, ansgeführt in den Jahren 1886 - 1893, Mitt. ans dem Mech. Techn. Lab. der K. Techn. Hochschule München, Heft 25, 1-19, 1897.

4. Griffith, A. A., The Phenomenon of Rupture and Flow in Solids, Phil. Trans. Roy. Soc. London, A 221, 163-198, 1920.

5. Kirsch, G., V.D.I. Vol. 42, 1898.

6. Coker, E. G., The Effects of Holes and Semi-Circular Notches on the Distribution of Stress in Tension Members Proc. Phys. Soc. 1912-1913, p.-95.

7. Coker, E. G., Chakko, K. C., and Satake, Y., Photoelastic and Strain Measurements of the Effects of Circular Holes on the Distribution of Stress in Tension Members, Proc. Instn. of Engrs. and Shipbuilders in Scotland, 1919-1920, p-34.

8. Preuss, E., V.D.I., No. 126, 1912 and No. 134, 1913.

9. Jeffery, G. B., Trans. Roy. Soc. (London), Series A, Vol. 221, p. 265, 1921.

10. Mindlin, R. D., Proc. Soc. Expl. Stress Analysis, Vol. 5, p. 56, 1948.

11. Howland, R. C. J., On the Stresses in the Neighbourhood of a Circular Hole in a Strip Under Tension, Phil. Trans. Roy. Soc. London A 229, p-49, 1929-1930.

12. Frocht, M. M., Photoelastic Studies in Stress Concentration, Mechanical Engineering, ASME, Volume 58, pp. 485-489, 1936.

13. Wahl, A. M., and Beeuwkes, R., Stress Concentration Produced

by Holes and Notches, Trans. ASME, Volume 56, pp.617-625, 1934.

14. Timoshenko, S., Journal of Franklin Institute, Vol. 197, p-505, 1924.

15. Timoshenko, S., Strength of Material, 2d ed., Vol. 2, p-317, D. Van Nostrand Company, Inc. N.Y.

16. Suzuki, Shin-Ichi, Stress Measurements in a Plate Containing a Reinforced Circular Hole using a Photoelastic Method, International Journal of Mechanical Sciences, p-473, 1964-65.

17. Howland, R. C. J., Stresses in a Plate containing an Infinite Row of Circular Holes, Proc. Roy. Soc. London A 148, 471-491, 1935.

18. Isida, M., On Some Plane Problems of an Infinite Plane Containing an Infinite Row of Circular Holes, Bull. JSME 3, 10, 259-265, May 1960, AMR 14 (1961), Rev. 2356.

19. Saito, H., Stress in a plate containing infinite parallel rows of holes, ZAMM 37, 3/4, 111-115, Mar./Apr. 1957; AMR 11(1958), Rev. 406.

20. Ling, C. B., The Stresses in a Plate Containing an Overlapped Circular Hole, J. Appl. Phys. 19, 405-411, Apr. 1948; AMR 1(1948), Rev. 784.

21. Ling, C. B., On the Stresses in a Plate Containing Two Circular Holes, J. Appl. Phys. 19, 77-82, Jan. 1948; AMR 1(1948), Rev. 411.

22. Borg, M. F., Maximum Stress Concentration Factors caused by Two Equal Circular Holes in a Plate Subjected to Uniform Axial Loading, David Taylor Model Basin Rep. 907, 13 pp., Sept. 1957; AMR 11(1958), Rev. 4911.

23. Atsumi, A., On the Stresses in a Strip Under Tension and Containing Two Equal Circular Holes Placed Longitidunally, J. Appl. Mech. 23, 555-562, 1956; AMR 11(1958), Rev. 82.

24. Ling, C. B., On Invariant Perforation in an Infinite Strip, Trans. ASME 81E(J. Appl. Mech.), 3, 422-431, Sept. 1959; AMR 13(1960), Rev. 2708.

25. Neuber, H., Kerbspannungslehre, Published by Julius Springer, Berlin, 1937, or Also Translation 24, David Taylor Model Basin, U.S. Navy Washington, D.C. November 1945; or Theory of Notch Stresses, J. W. Edwards, Publisher, Inc., Ann Arbor, Mich, 1946.

26. Seely, F. B., and Smith, J. O. Advanced Mechanics of Materials, John Wiley & Sons, Inc., New York, 1959.

27. Ford, H., Advanced Mechanics of Materials, John Wiley & Sons, Inc., N. Y.

28. Babuska, I., and Kautsky, J., Optimization of Notch Shapes (in German), ZAMM 43, 1/2, 47-54, Jan./Feb. 1963; AMR 17 1964), Rev. 1979.

29. Hahn, H. G., The Influence of Notch Angles on Stress Concentration (in German), Acta Mechanica 1, 1-15, 1965; AMR 18(1965), Rev. 6606.

30. Ling, C. B., Stresses in a Notched Strip Under Tension. J. Appl. Mech. 14, 275-280, Dec. 1947; AMR 1(1948), Rev. 230.

31. Peterson, R. E., Stress in a Notched Strip Under Tension, Discussion of Reference [26], J. Appl. Mech. 15, p-176, 1948.

32. Frocht, M. M., Guernsey, R., Jr., and Landsberg, D., A Photoelastic Re-examination of Notched Tension Bars, J. Appl. Mech. 19, p-124, March 1952; AMR 5(1952), Rev. 3044.

33. Isida, M., Form Factors of a Strip with Semicircular Notches in Tension and Bending Sci. Pap. Fac. Engng., Tokushima Univ. 4, 67-68, 1953.

34. Atsumi, A., Stress Functions for an Infinite Strip with Semicircular Notches (Japanese) Trans. Japan Soc. Mech. Engrs. 20, 699-706, 1954.

35. Coker, E. G., and Heymans, P., Stress Concentrations due to Notches and like Discontinuities, Brit. Ass. Rep. 1921, 291-299.

36. Brown, A. F. C., and Hickson, V. M., Photoelastic Investigation of the Stress Concentration Caused by Surface Irregularities, Proc. 7th Internat. Congr. Appl. Mech., Vol. 1 (1948), pp. 269-279.

37. Frocht, M. M., and Landsberg, D., Factors of Stress Concentration in Bars With Deep Sharp Grooves and Fillets in Tension, Proc. SESA, Volume 8, No. 2, pp. 149-162, 1951, AMR 4(1951), Rev. 3174.

38. Frocht, M. M., A Photoelastic Investigation of Stress Concentrations due to small Fillets and Grooves in Tension, NACA TN-2442, 45 pp., Aug. 1951; AMR 5(1952), Rev. 368.

39. Frocht, M. M., and Leven, M. M. Factors of Stress Concentration for Slotted Bars in Tension and Bending, J. Appl. Mech. 18, 1, 107-108, Mar. 1951; AMR 4(1951), Rev. 2385.

40. Shimada, H., Photoelastic Investigation of Stresses in Bars with Reinforced Semicircular Notches under Bending, Proc. SESA, Vol. 19, No. 1, p-75.

41. Murakami, Y., and Kawabe, T., Photoelastic Study of Flat Bars with a Double Notch on one Edge subjected to Pure Bending, JSME 1961, Vol. 4, No. 15, p-470.

42. Nishihara, T., and Fuji, T., Reduction of Stress Concentration by Additional Notches, Proc. Japan Nat. Congr. Appl. Mech. 4, 215-218, 1954.

43. Thum, A., and Berg, S., Die Entlastungskerbe, Forsch. Ing. Wes. 2, 345-351, 1931.

44. Okubo, H., Die Formzahlen bei Entlastungskerben, JSME 62, 1272-1276, 1959.

45. Durelli, A. J., Lake, R. L., and Phillips, E., Stress Concentrations Produced by Multiple Semicircular Notches in Infinite Plates Under Uniaxial State Stress, Proc. SESA, Vol. 10, No. 1, pp. 53-64, 1952; AMR 6(1953), Rev. 1527.

46. Nishioka, K., and Hisamitsu, N., On the Stress Concentration in Multiple Notches, J. Appl. Mech. 29, 575-577, 1962.

47. Thum, A., and Svenson, O., Beauspruchung bei mehrfacher kerbwirkung, Entlastungs - and Überlastungskerben, Schweiz. Arch. 15, 161-174, 1949; AMR 3(1950), Rev. 1643.

48. Thum, A., and Svenson, O., Mehrfache Kerbwirkung, Entlastungskerben - Überlastungskerben, Z. VDI 92, 225 - 230, 1950.

49. Paul, F. W. Jr., and Faucett, T. R., The Superposition of Stress Concentration Factors, Trans. ASME 84B (J. Engng. Indust.) 1, 129-134, Feb. 1962; AMR 15(1962), Rev. 5271.

50. Vicentini, V., Stress Concentration Factors for superposed Notches. Experimental Mechanics 7, 1967 (March).

51. Shanley, F. R., Strength of Materials, McGraw-Hill Book Company, Inc., N. Y. 1957.

52. Frocht, M. M., Photoelasticity, Vol. I, II, John Wiley and Sons, Inc., N. Y.

53. Roylance, T.F., Engineering Design, Symposium Publications Division, Pergamon Press, London, 1st ed., 1966.

54. Maleev, V. L., Machine Design, International Text Book Company, Scranton, Pennsylvania, 1st ed. sixth Printing Oct. 1946.

55. Spotts, M. F., Design of Machine Elements, Prentice-Hall, Inc. N. Y., 2nd ed. 1953.

56. Richards, C. W., Engineering Materials Science, Wadsworth Publishing Company, Inc., Belmont, California.

57. Coker, E. G., and Filon, L. N. G., A. Treatise on Photo-Elasticity, Cambridge University Press, 1931.

58. Lee, G. H., An Introduction to Experimental Stress Analysis, John Wiley and Sons, Inc., N. Y.

59. Durelli, A. J.,Phillips, E. A., and Tsao, G. H., Introduction to the Theoretical and Experimental Analysis of Stress and Strain, McGraw-Hill Book Company, Inc. N.Y.

60. Hetenyi, M., Handbook of Experimental Stress Analysis, John Wiley and Sons, Inc. N. Y.

61. Durelli, A. J., and Riley, W.F., Introduction to Photomechanics, Prentice-Hall, Inc., N. J.

62. Dally, J. M., and Riley, W. F., Experimental Stress Analysis, McGraw-Hill Book Company, Inc.

63. Timoshenko, S. and Goodier, J. N., Theory of Elasticity, 2nd ed., McGraw-Hill Book Co., Inc.

64. Roark, R. J., Formulas for Stress and Strain, McGraw-Hill Book Company, N. Y. 4th ed.

65. Smith, C. R., Design Tips for Preventing Fatigue Failures, Part 1, Assembly Engineering, March, April and May, 1968, copyright 1968 by Hitchcock Publishing Company, Wheaton, Illinois.

APPENDICES

APPENDIX A

ADJUSTMENTS OF THE DIFFUSED LIGHT POLARISCOPE

The constructional details of the Diffused Light Polariscope are available in standard reference or text books [61, 62] dealing with photoelastic stress analysis. However, Figure A.1 depicts the photographic view of the diffused light polariscope used in the laboratory for carrying out the present experiment.

The major elements of importance are Polarizer, Analyser, First quarter wave ($\frac{\lambda}{4}$) plate, second quarter wave plate. All these elements must be set in their relative positions in a specific manner as to give rise to the proper formation of the circularly polarized light necessary for the production of isochromatic fringe patterns. So the following essential steps were taken for proper adjustment of the elements, before the actual testing of the models.

Polarizer and Analyzer

1. The plane of polarization was set to 0°
2. Both $\frac{\lambda}{4}$ plates were removed.
3. While the polarizer was kept fixed, with the plane of polarization set at 0°, the analyzer was rotated until extinction was achieved. In this position the axis of the polarizer and analyzer were crossed and corresponded to a dark field arrangement. The polarizer and analyzer were locked in this position.

4. The plane of polarization of the polarizer was made vertical by fixing a plastic tension specimen in the loading frame such that it was vertical and under a tensile load. Viewing in white light, rotated the polarizer and analyzer in their locked together configuration until maximum extinction occurred in the model. This implied that the axis of polarization of the polarizer was vertical.

First Quarter Wave Plate

5. The $\frac{\lambda}{4}$ plate was inserted adjacent to the polarizer in the polariscope assembly.
6. Rotated the $\frac{\lambda}{4}$ plate until extinction occurred. This meant that one of the axis of the $\frac{\lambda}{4}$ plate became vertical and coincided with the axis of the polarizer. The plate was then rotated 90 degrees until extinction occurred again. The $\frac{\lambda}{4}$ plate was rotated back 45 degrees and locked to the polarizer.
7. The plate was then removed.

Second Quarter Wave Plate

8. The second $\frac{\lambda}{4}$ plate was inserted and the procedure used for the first $\frac{\lambda}{4}$ plate was repeated.
9. The first $\frac{\lambda}{4}$ was set back into the polariscope and aligned in its previously determined position. Extinction could occur, but did not, and therefore rotated one of the $\frac{\lambda}{4}$ plates 90 degrees from its original position. Extinction occurred.

10. The above adjustments of the polarizer, analyzer and $\frac{\lambda}{4}$ plates resulted in the field of circularly polarized light necessary to observe the isochromatic fringe patterns.

Figures A.2 a,b show the settings of various elements in a diagramatic view.

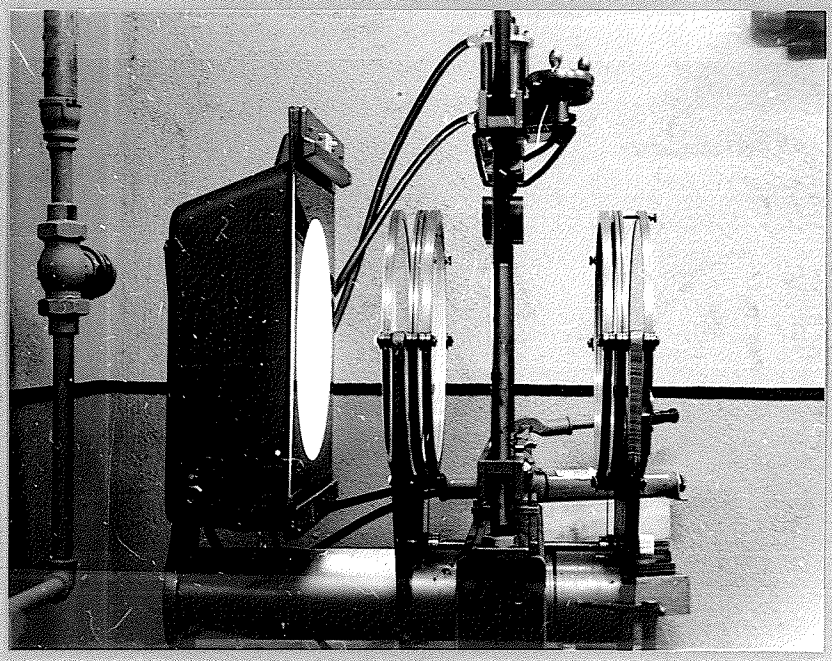

Figure A.1 Photographic View of Position of Elements in a Diffused Light Type Polariscope in the Laboratory.

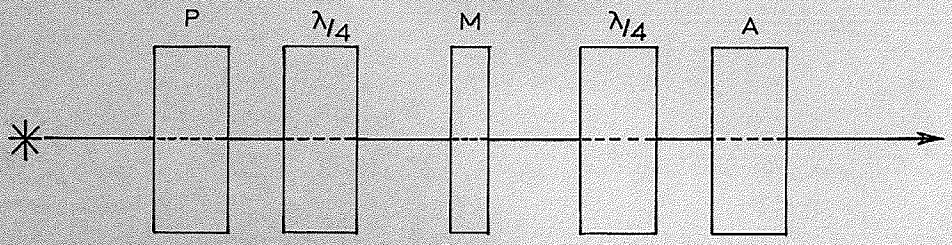

(a) Position of Elements Viewed Perpendicular to Axis of Propagation.

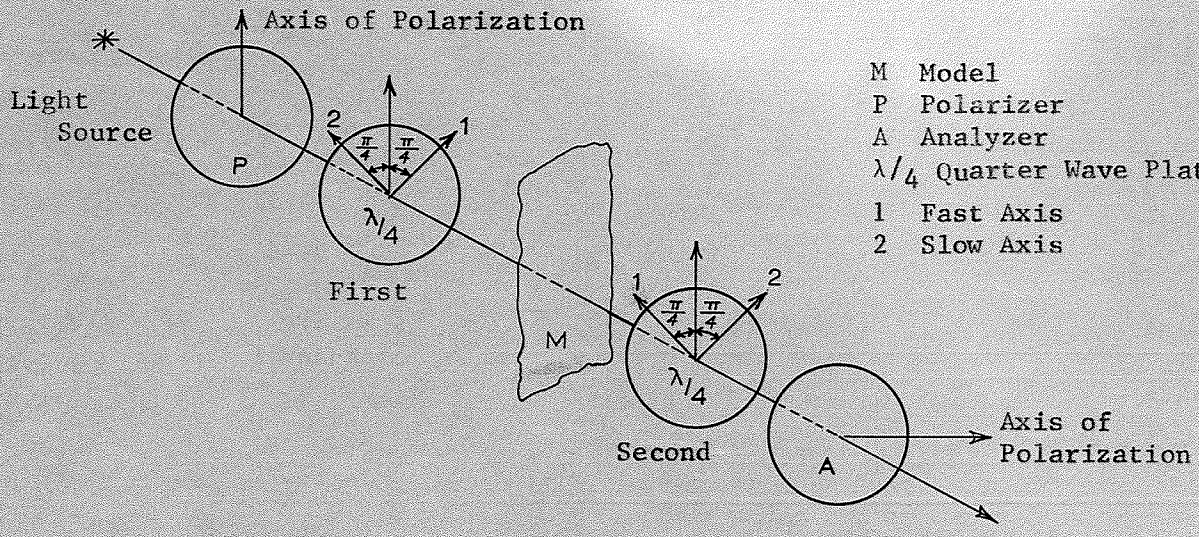

(b) Position of Elements Viewed through the Analyzer along the Axis of Propagation.

Figure A.2 Diagramatic Setting of Elements of Circular Polariscope.

APPENDIX B

CALIBRATION OF PHOTOELASTIC MATERIAL

The material fringe values of photoelastic materials vary with the supplier, the batch of resin, temperature, and age. For this reason, it is always necessary to calibrate each sheet of photoelastic material at the time of test.

Therefore, a model conforming to the dimensions of a tension specimen shown in Figure 4.1 was machined on the router with all the necessary precautions, out of a sheet of photoelastic material PSM-1. It was loaded in tension in the field of circular polariscope. The readings of the load (applied in increments), varying with the increasing fringe order were recorded and a straight line graph drawn between them is shown in Figure B.1

For a shank width B and a thickness h of the tensile specimen, the axial stress induced in the shank by the load P may be expressed as

$$\sigma_1 = \frac{P}{Bh} \quad \text{and} \quad \sigma_2 = 0 \qquad \text{(A-1)}$$

Substituting equations A-1 into equation 3-3 gives

$$\frac{P}{Bh} = \frac{Nf_\sigma}{h} \quad \text{or} \quad f_\sigma = \frac{P}{BN}$$

But, B = 1 inch.

Therefore, $f_\sigma = \frac{P}{N}$

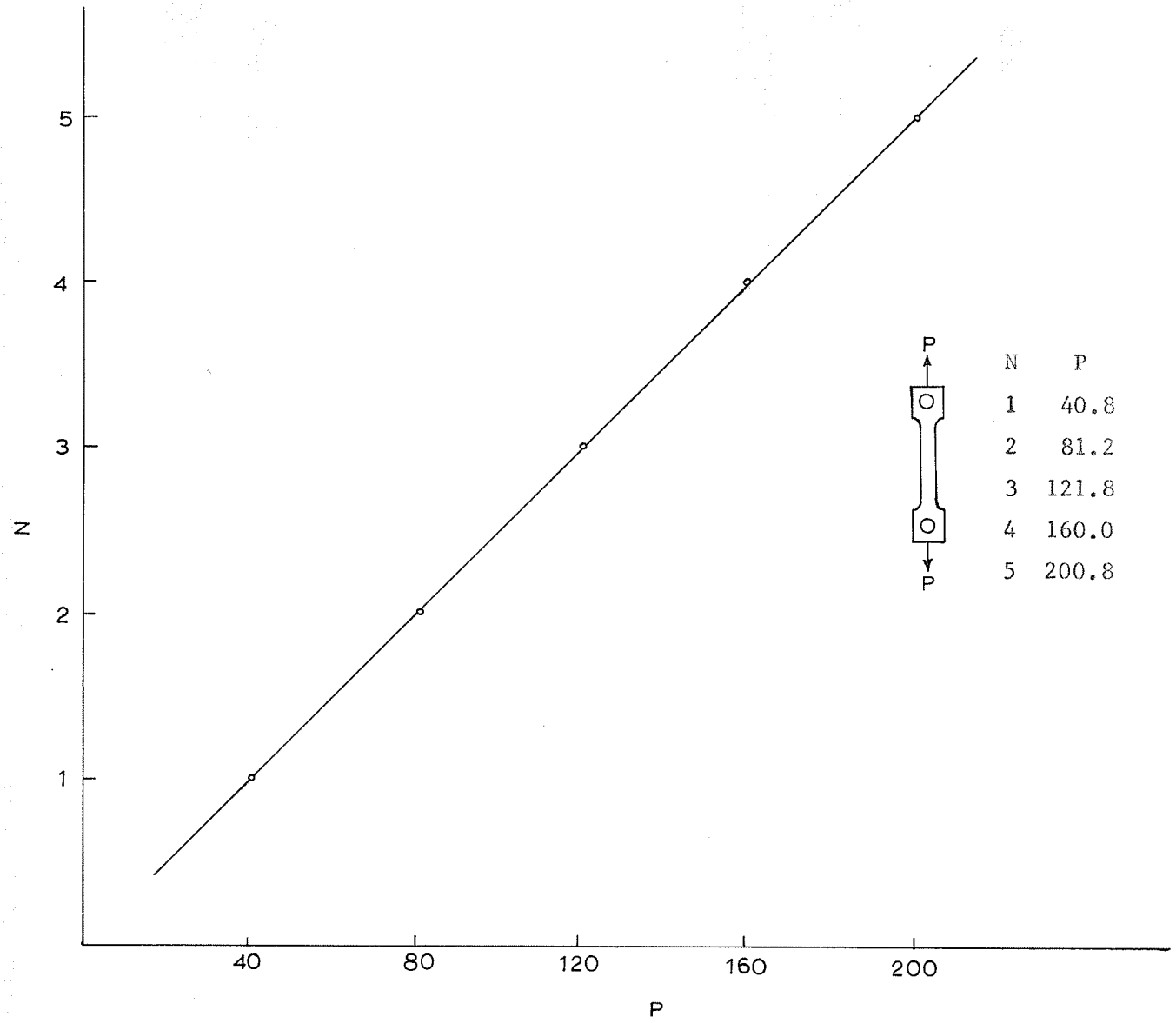

Figure B.1 Variation of Fringe Order N with Applied Load P in Un-notched Tension Model.

Value $P/_N$ is given by the slope of the straight line graph of Figure B.1. It was observed from the slope, that $\frac{P}{N} = 40.05$

Thus the calibrated material fringe value,

$$f_\sigma = 40.05 \text{ psi} - \text{in}/_{\text{fringe}}.$$

APPENDIX C

SAMPLE CALCULATIONS

Sample Calculations for case of Precise Measurement:

Maximum Stress

using relation 3-5

$$\sigma_{max} = NF = N_{max} \frac{f_\sigma}{h}$$

where F = Model fringe value, $psi/_{fringe}$.

f_σ = Material fringe value, psi - $in/_{fringe}$.

= 40.05 psi-$in/_{fringe}$ (calibrated value).

h = Thickness of model = ¼ in.

N = Maximum fringe order at the point of stress concentration on the boundary of discontinuity = N_{max}

= Fractional fringe order for unit load as entered in Table 5-1.

Model H_{10} $\frac{N}{P} = \frac{1}{12.30}$ (Table 5-1)

For arbitrary load, P = 100 lb, $N = \frac{100}{12.3}$

$$\sigma_{max} = \frac{100}{12.3} \times \frac{40.05}{\frac{1}{4}} = \underline{1302 \text{ psi.}}$$ (Table 5-2)

Model H_{21}

For Stress Raiser, $\frac{N}{P} = \frac{1}{12.00}$ (Table 5-1)

$$\sigma_{max} = \frac{100}{12.00} \times \frac{40.05}{\frac{1}{4}} = \underline{1332.50 \text{ psi}}$$ (Table 5-2)

For Stress Reducer, $\frac{N}{P} = \frac{1}{34.00}$ (Table 5-1)

$\sigma_{max} = \frac{100}{34} \times \frac{40.05}{\frac{1}{4}} = \underline{471.00 \text{ psi}}$ (Table 5-2)

Model N_{32}

For Stress Raiser, $\frac{N}{P} = \frac{1}{10.6}$ (Table 5-1)

$\sigma_{max} = \frac{100}{10.6} \times \frac{40.05}{\frac{1}{4}} = \underline{1510.00 \text{ psi}}$ (Table 5-3)

For Stress Reducer, $\frac{N}{P} = \frac{1}{17.375}$ (Table 5-1)

$\sigma_{max} = \frac{100}{17.375} \times \frac{40.05}{\frac{1}{4}} = \underline{922.00 \text{ psi}}$ (Table 5-3)

Stress Concentration Factor

using relation 3-6

$$K_t = \frac{\sigma_{max}}{\sigma_{nom}} = \frac{Nf_{\sigma/h}}{P/A} = \frac{N_{max} \; f_{\sigma/h}}{P/bh}$$

where b = Net width of shank of Tension Specimen

= B - d

d being the depth of discontinuity i.e., diameter in case of hole and depth in case of notch

B = 1 inch for all models

$K_t = \frac{N_{max}}{P} (1-d) f_\sigma$ (C - 1)

Model H_{10}

$K_t = \frac{1}{12.30} (1 - \frac{5}{16}) 40.05 = \underline{2.237}$ (Table 5-2)

Model H_{21}

For Stress Raiser,

$$K_t = \frac{1}{12.00}\left(1 - \frac{5}{16}\right) 40.05 = \underline{2.293} \qquad \text{(Table 5-2)}$$

For Stress Reducers,

$$K_t = \frac{1}{34.00}\left(1 - \frac{1}{16}\right) 40.05 = \underline{1.102} \qquad \text{(Table 5-2)}$$

Model N_{32}

For Stress Raiser,

$$K_t = \frac{1}{10.60}\left(1 - \frac{5}{16}\right) 40.05 = \underline{2.593} \qquad \text{(Table 5-3)}$$

For Stress Reducer,

$$K_t = \frac{1}{17.375}\left(1 - \frac{1}{16}\right) 40.05 = \underline{2.016} \qquad \text{(Table 5-3)}$$

Sample Calculations for case of Extrapolation:

With reference to fringe orders $N = N_M - N_O$ under a net load $P = P_M - P_O$ as listed in Table 5-5, the values of σ_{max} and K_t were calculated. The values of σ_{max} were also calculated for arbitrary load of 100 lb. for purposes of comparison with the corresponding values found by precise measurement method. The above said values are listed in Table 5-6. Few sample calculations are given as below.

Maximum Stress

using relation 3-5

$$\sigma_{max} = NF = N_{max} \frac{f_\sigma}{h}$$

Model H_{10}

For Stress Raiser

Under net load, $P = P_M - P_O = 88$ lb, the fringe order

$N = N_{max} = N_M - N_o = 6.2$ (Table 5-5)

$\sigma_{max} = 6.2 \times \frac{40.05}{\frac{1}{4}} = \underline{993.00 \text{ psi}}$ (Table 5-6)

Model H_{24}

For Stress Raiser, $N = 6.0$ (Table 5-5)

under net load, 88 lb, $\sigma_{max} = 6.0 \times \frac{40.05}{\frac{1}{4}}$

$= \underline{962.00 \text{ psi}}$ (Table 5-6)

under load, 100 lb, $\sigma_{max} = \frac{962.00}{88} \times 100$

$= \underline{1092.5 \text{ psi}}$ (Table 5-6)

For Stress Reducer, $N = 5.4$ (Table 5-5)

under net load 88 lb, $\sigma_{max} = 5.4 \times \frac{40.05}{\frac{1}{4}}$

$= \underline{865.00 \text{ psi}}$ (Table 5-6)

under load, 100 lb, $\sigma_{max} = \frac{865.00}{88} \times 100$

$= \underline{983.00 \text{ psi}}$ (Table 5-6)

Stress Concentration Factor

using relation C - 1

$$K_t = \frac{N_{max}}{P}(1 - d) f_\sigma = \frac{\frac{N_{max}}{P}}{(1-d)f_\sigma}$$

or

$$K_t = \frac{N_{max}}{N_{nom}} \quad \text{where} \quad N_{nom} = \frac{P}{(1-d)f_\sigma}$$

$$P = P_M - P_O$$

and $$N_{max} = N = N_M - N_O$$

Model H_{10}

(Table 5-5)

$$N_{max} = 6.2$$

$$N_{nom} = \frac{88}{(1 - \frac{5}{16})\ 40.05} = 3.199$$

(Table 5-6)

$$K_t = \frac{6.2}{3.199} = \underline{1.937}$$

Model N_{22}

For Stress Raiser

(Table 5-5)

$$N_{max} = 8.0$$

$$N_{nom} = \frac{88}{(1 - \frac{5}{16})\ 40.05} = 3.199$$

(Table 5 - 6)

$$K_t = \frac{8}{3.199} = \underline{2.5}$$

For Stress Reducer

$N_{max} = 4.0$ (Table 5-5)

$$N_{nom} = \frac{88}{(1 - 1/8)\ 40.05} = 2.512$$

$$K_t = \frac{4.0}{2.512} = 1.593$$ (Table 5-6)